

Training Fully Connected Neural Networks is $\exists\mathbb{R}$ -Complete

Daniel Bertschinger¹, Christoph Hertrich², Paul Jungeblut³, Tillmann Miltzow⁴, and Simon Weber⁵

¹Department of Computer Science, ETH Zurich, daniel.bertschinger@inf.ethz.ch

²Department of Mathematics, London School of Economics, c.hertrich@lse.ac.uk

³Institute of Theoretical Informatics, Karlsruhe Institute of Technology, paul.jungeblut@kit.edu

⁴Department of Information and Computing Sciences, Utrecht University, t.miltzow@uu.nl

⁵Department of Computer Science, ETH Zurich, simon.weber@inf.ethz.ch

Abstract

We consider the algorithmic problem of finding the optimal weights and biases for a two-layer fully connected neural network to fit a given set of data points. This problem is known as *empirical risk minimization* in the machine learning community. We show that the problem is $\exists\mathbb{R}$ -complete. This complexity class can be defined as the set of algorithmic problems that are polynomial-time equivalent to finding real roots of a polynomial with integer coefficients. Our results hold even if the following restrictions are all added simultaneously.

- There are exactly two output neurons.
- There are exactly two input neurons.
- The data has only 13 different labels.
- The number of hidden neurons is a constant fraction of the number of data points.
- The target training error is zero.
- The ReLU activation function is used.

This shows that even very simple networks are difficult to train. The result offers an explanation (though far from a complete understanding) on why *only* gradient descent is widely successful in training neural networks in practice. We generalize a recent result by Abrahamsen, Kleist and Miltzow [NeurIPS 2021].

This result falls into a recent line of research that tries to unveil that a series of central algorithmic problems from widely different areas of computer science and mathematics are $\exists\mathbb{R}$ -complete: This includes the art gallery problem [JACM/STOC 2018], geometric packing [FOCS 2020], covering polygons with convex polygons [FOCS 2021], and continuous constraint satisfaction problems [FOCS 2021].

Acknowledgments. Christoph Hertrich is supported by the European Research Council (ERC) under the European Union’s Horizon 2020 research and innovation programme (grant agreement ScaleOpt-757481). Tillmann Miltzow is generously supported by the Netherlands Organisation for Scientific Research (NWO) under project no. 016.Veni.192.250. Simon Weber is supported by the Swiss National Science Foundation under project no. 204320.

1 Introduction

The usage of neural networks in modern computer science is ubiquitous. It is arguably the most powerful tool at our hands in machine learning [40]. Two impressive applications are in the generation of photo-realistic pictures as well as in AI systems that can beat humans in the game of Go, see Figure 1.

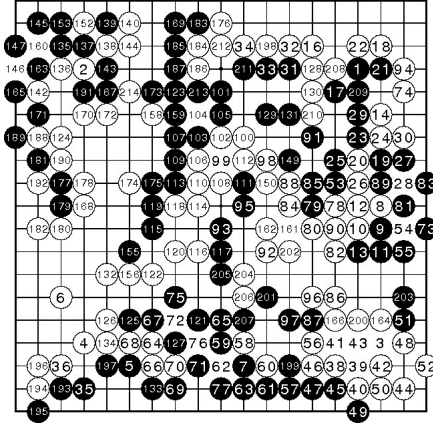


Figure 1: Left: A computer generated picture [63] (public domain). Right: Game of Go by AlphaGo vs. Fan Hui [6] (licensed under CC BY-SA 4.0).

One of the arguably most fundamental algorithmic questions asks for the algorithmic complexity to actually train a neural network. For arbitrary network architectures, Abrahamsen, Kleist and Miltzow [3] showed that the problem is $\exists\mathbb{R}$ -complete already for two-layer neural networks and linear activation functions. The complexity class $\exists\mathbb{R}$ is defined as the family of algorithmic problems that are polynomial-time equivalent to finding real roots of polynomials with integer coefficients. See Section 1.3 for a proper introduction. This result is interesting for two main reasons.

- Mathematical curiosity about a central problem in computer science.
- The $\exists\mathbb{R}$ -hardness gives a partial explanation on why *only* gradient descent has been successful in training neural networks in practice.

The result by Abrahamsen, Kleist and Miltzow [3] has one major downside. Namely, the network architecture is *adversarial*: The hardness result inherently relies on choosing a network architecture that is particularly difficult to train. The instances by Abrahamsen, Kleist and Miltzow could be trivially trained with fully connected neural networks, as they reduce to matrix factorization. This stems from the fact that they use the identity function as the activation function. While intricate network architectures (for example, convolutional and residual neural networks, pooling, autoencoders, generative adversarial neural networks) are common in practice, they are usually designed in a way that facilitates training rather than making it difficult [40]. Here, we strengthen the result in [3] by showing hardness for *fully connected* two-layer neural networks. This shows that $\exists\mathbb{R}$ -hardness does not stem from an adversarial network architecture but is **inherent in the neural network training problem** itself. Although in practice a host of different architectures are used, fully connected two-layer neural networks are arguably the most basic ones and they are often part of more complicated network architectures [40]. We can show hardness even for the most basic case with the following properties:

- There are exactly two input neurons.
- There are exactly two output neurons.
- The data has only 13 different labels.
- The number of hidden neurons is a constant fraction of the number of data points.
- The target training error is zero.
- The ReLU activation function is used.

In the following, we give different perspectives on how to interpret our findings. Then, we present precise definitions and state our results formally. This is the basis for an in-depth discussion of the strength and limitations from different perspectives. Thereafter we give an introduction to related work on $\exists\mathbb{R}$ -completeness and theory on neural networks. We finish the introduction by giving the key ingredients of the proof of our result.

Implications of $\exists\mathbb{R}$ -Completeness. Proving $\exists\mathbb{R}$ -completeness of a problem that is already known to be **NP**-hard is a valuable contribution for at least two reasons: Firstly, from a theoretical standpoint we are always interested in the exact complexity of an algorithmic problem. Secondly, $\exists\mathbb{R}$ -completeness provides a better understanding of the difficulties that need to be overcome when designing algorithms for the considered problem: While there is a wide collection of extremely optimized off-the-shelf tools like SAT- or ILP-solvers applicable to many **NP**-complete problems, no such general purpose tools are available for $\exists\mathbb{R}$ -complete problems. The reason for this is their continuous solution space as well as the inherent nonlinear relations between their variables. Attempts to discretize the solution space had only limited success [45, 55]. As an illustrative example of the practical difficulties, consider the $\exists\mathbb{R}$ -complete problem of packing unit-squares into a square container [4]: Figure 2 shows how to optimally pack five unit-squares into a minimum square container and the best known (but potentially not optimal) way to pack eleven unit-squares.

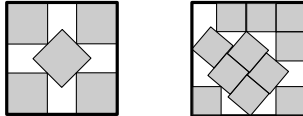


Figure 2: Left: Packing of five unit squares into a minimum square container. Right: The best known packing of eleven unit squares into a square container [34]. This is not known to be optimal.

One method that can often be used to get approximate solutions for $\exists\mathbb{R}$ -complete problems is gradient descent. Note that this also applies in the context of training neural networks, where a bunch of different gradient descent variants powered by backpropagation are widely used. However, when using gradient descent we usually do not get any guarantees on the quality of the obtained solutions or the time it takes to compute them. Thus it would be very desirable to use other methods, like SAT- or ILP-solvers that are reliable and terminate in exponential (but finite) time. $\exists\mathbb{R}$ -completeness indicates that this may not be feasible.

Let us stress that $\exists\mathbb{R}$ -completeness does not rule out any hope for good heuristics. Other $\exists\mathbb{R}$ -complete problems like the art gallery problem can be solved in practice via custom heuristics, sometimes also in combination with ILP-solvers [22]. Under additional assumptions, those methods are even shown to work reliably [45]. Thus, $\exists\mathbb{R}$ -completeness of training neural networks does not exclude the possibility of appropriate assumptions that make training tractable. Assumptions are appropriate if they are mathematically natural and related to practice. For instance, if there is only one output neuron, it is possible to train two-layer neural networks to global optimality [7].

Relation to Previous Results. It is a well-known fact that minimizing the training error of a neural network is a computationally hard problem for a large variety of activation functions and architectures [75]. For ReLU networks, NP-hardness, parameterized hardness, and inapproximability results have been established even for the simplest possible architecture consisting of only a single ReLU neuron [15, 24, 32, 38]. On the positive side, the seminal algorithm by Arora, Basu, Mianjy, and Mukherjee [7] solves empirical risk minimization for 2-layer ReLU networks and one-dimensional output to global optimality. It was later extended to a more general class of loss functions by Froese, Hertrich, and Niedermeier [32]. The running time is exponential in the number of neurons in the hidden layer and in the input dimension, but polynomial in the number of data points if the former two parameters are considered to be a constant. In particular, this algorithm implies that the problem is contained in NP. The idea is to perform a combinatorial search over all possible activation patterns (whether the input to each ReLU is positive or negative). Since then, a generalization of this algorithm to more complex architectures has been highly desired. Our result now yields an explanation why no such algorithm has been found: adding only a second output neuron to the architecture considered by Arora et al. [7] makes empirical risk minimization $\exists\mathbb{R}$ -hard, implying that a combinatorial search algorithm of that flavor cannot exist unless $\text{NP} = \exists\mathbb{R}$.

Relation to Learning Theory. In this paper we purely focus on the computational complexity of empirical risk minimization, that is, minimizing the *training error*. In the machine learning practice, one usually desires to achieve low *generalization error*, which means to use the training data to achieve good predictions on unseen test samples.

To formalize the concept of the generalization error, one needs to combine the computational aspect with a statistical one. There are various models to do so in the literature, the most famous one being *probably approximately correct* (PAC) learnability [75, 81]. While empirical risk minimization and learnability are two different questions, they are strongly intertwined. We will provide more details about these interconnections when we discuss further related literature.

Despite the close connections between empirical risk minimization and learnability, to the best of our knowledge, the $\exists\mathbb{R}$ -hardness of the former has no direct implications on the complexity of the latter. Still, since empirical risk minimization is the most common learning paradigm in practice, our work is arguably also interesting in the context of learning theory.

1.1 Definitions and Results.

In order to describe our results, we need to introduce the standard definitions concerned with the type of neural networks studied by us.

Definition 1 (Neural Network). A *neural network* is a directed acyclic graph $N = (V, E)$ (the *architecture* or *netowrk*) with edge weights $w_{uv} \in \mathbb{R}$ for each $uv \in E$. The vertices of N are called *neurons*. The neurons $S \subseteq V$ with in-degree zero are called *inputs*, similarly the neurons $T \subseteq V$ with out-degree zero are called *outputs*. All other neurons are *hidden neurons*. Additionally there is a bias $b_v \in \mathbb{R}$ and an activation function φ_v for each hidden neuron $v \in V \setminus (S \cup T)$.

The vertices can be partitioned into layers $V = V_0 \cup \dots \cup V_{k+1}$ where $S = V_0$ and $T = V_{k+1}$, such that each edge goes from V_i to V_{i+1} . The layers V_1, \dots, V_k are called *hidden layers*. The neural network is *fully connected* if it contains exactly all possible edges between two consecutive layers. The probably most commonly used activation function [7, 35, 40] is the *rectified linear unit* (ReLU) defined as $\text{ReLU} : \mathbb{R} \rightarrow \mathbb{R}, x \mapsto \max\{0, x\}$.

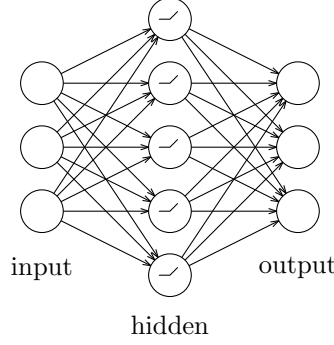


Figure 3: A neural network is defined as a directed acyclic graph. Sources and sinks are called input and output neurons. The symbol inside the hidden neurons expresses the ReLU activation function.

In case that there is only one hidden layer, we speak (confusingly) of a *two-layer* neural network. The name stems from the interpretation that there are two layers of edges, even though the vertex set is split into three layers.

Given a neural network architecture N as defined above, assume that we fixed an ordering on S and T . Then N realizes a function $f(\cdot, \Theta) : \mathbb{R}^{|S|} \rightarrow \mathbb{R}^{|T|}$, where Θ denotes the weights and biases that parameterize the function. For $x \in \mathbb{R}^{|S|}$ we define $f(\cdot, \Theta)$ inductively: The i -th input neuron forwards the i -th component of x to all its outgoing neighbors. Each hidden neuron forms the weighted sum over all incoming values, adds its bias, applies the activation function to this sum and forwards it to all outgoing neighbors. An output neuron again forms the weighted sum over all incoming values but does not add a bias and does not apply any activation function.

Note that it is possible to also use ReLUs for the output neurons. Here we restrict ourselves to the case that ReLUs are only used for hidden neurons, as we do not want to confuse the reader by considering too many variants of two-layer neural networks. Architectures with ReLUs on the output neurons seem to be less commonly used in practice [40], but we believe that our proofs could also be adapted to this case.

We introduced neural networks using the language of graphs. We want to point out that this is only one possible perspective. Fully connected neural networks can also be described as the alternating composition of affine/linear functions and the (componentwise) ReLU function.

Definition 2 (TRAIN-F2NN). We define the problem of training a fully connected two-layer neural network (TRAIN-F2NN) to be the following decision problem:

Input: A 4-tuple (m, D, γ, c) where

- $m \in \mathbb{N}$ encoded in unary is the size of the hidden layer,
- D is a set of n data points of the form $(x; y) \in \mathbb{Q}^{|S|} \times \mathbb{Q}^{|T|}$,
- $\gamma \in \mathbb{Q}_{\geq 0}$ is the target error and
- $c : \mathbb{R}^{|T|} \times \mathbb{R}^{|T|} \rightarrow \mathbb{R}_{\geq 0}$ is the loss function.

Question: Are there weights and biases Θ such that $\sum_{(x;y) \in D} c(f(x, \Theta), y) \leq \gamma$?

The reason to encode m in unary is to guarantee that the described neural network has size polynomial in the input size. Furthermore, we assume that the loss function is *honest*, meaning that it returns zero if and only if the data is fit exactly. We will see that this is the only required assumption on the loss function to prove $\exists\mathbb{R}$ -hardness of the zero-error case. To prove $\exists\mathbb{R}$ -membership, we further assume that the loss function can be computed in polynomial time on the real RAM.

We are now ready to state our main result.

Theorem 3. *The problem TRAIN-F2NN is $\exists\mathbb{R}$ -complete, even if:*

- *There are exactly two input neurons.*
- *There are exactly two output neurons.*
- *The number of hidden neurons is a constant fraction of the number of data points.*
- *The data has only 13 different labels.*
- *The target error is $\gamma = 0$.*
- *The ReLU activation function is used.*

1.2 Discussion

In this section, we discuss our main theorem from various perspectives, pointing out strengths and limitations. This includes, but is not limited to, identifying angles from which it is tight and angles from which it leaves room for further research.

Input Neurons. In practice, neural networks are often trained on high dimensional data, thus having only two input neurons is even more restrictive than the practical setting. Note that we easily obtain hardness for higher input dimensions by simply placing all data points of our reduction into a two-dimensional subspace. The precise complexity of training fully connected two-layer neural networks with only one-dimensional input and multi-dimensional output remains unknown. While this setting does not have practical relevance, we are still curious about this open question from a purely mathematical perspective.

Output Neurons. If there is only one output neuron instead of two, then the problem is known to be contained in NP [7]. See also the discussion about the related work above. Thus, unless $\text{NP} = \exists\mathbb{R}$, our result cannot be improved further in terms of the number of output neurons.

Hidden Neurons. Consider the situation that the number m of hidden neurons is larger than the number n of data points. If there are no two contradicting data points with $x_i = x_j$ but $y_i \neq y_j$, then it is known that we can always fit all the data points [85]. Thus, having a linear number of data points in terms of m is the fewest possible we can expect. We wonder whether it is possible to show $\exists\mathbb{R}$ -completeness with $n \leq (1 + \varepsilon)m$ for every fixed ε .

Output Labels. The number of labels used in our reduction is the small constant 13. A small set of possible labels shows relevance of our results to practice, where we are often confronted with a large number of data points but a much smaller number of labels, for instance, in classification tasks. The set of labels used by us is

$$\{(-2, 6), (-1, -1), (-1, 0), (0, -1), (0, 0), (0, 3), (2, 2), (3, 3), (3, 6), (4, 4), (6, -2), (6, 6), (11, 11)\}.$$

If all labels are contained in a one-dimensional affine subspace the problem is in NP, as then they can be projected down to one-dimensional labels and the problem can be solved with the algorithm by Arora et al. [7]. As any two labels span a one-dimensional affine subspace, $\exists\mathbb{R}$ -hardness can only be achieved with at least three (affinely independent) output labels.

We are not particularly interested in closing the gap between 13 and 3 output labels, but it would be interesting to investigate the complexity of the problem when output labels have more structure. For example, in classification tasks one often uses *one-hot encodings*, where for k classes, a k -dimensional output space is used and all labels have the form $(0, \dots, 0, 1, 0, \dots, 0)$. Note that in this case, at least three output dimensions are needed to obtain three different labels.

Target Error. We show hardness for the case with target error $\gamma = 0$. Arguably, it is often not required in practice to fit the data exactly. It is not too difficult to see that, under mild conditions on the loss function, we can easily modify the value of γ by adding inconsistent data points that can only be fit best in exactly one way. Thus, for different values of γ , the decision problem does not get easier.

Activation Functions. Let us point out that the ReLU activation function is currently still the most commonly used activation function in practice [7, 35, 40]. Our methods are probably easily adaptable to other piecewise linear activation functions, for example, leaky ReLUs. Having said that, our methods are not applicable to other types of activation functions at all. For example, Sigmoid, soft ReLU or step functions. We want to point out that TRAIN-F2NN (and even training of arbitrary other architectures) is in NP in case a step function is used as the activation function [51]. For the Sigmoid and soft ReLU function it is not even clear whether the problem is decidable, as trigonometric functions and exponential functions are not computable on the real RAM [31, 66].

Lipschitz Continuity and Regularization. The set of data points created in the proof of Theorem 3 is intuitively very tame. To make this more precise, our reduction fulfills the following property: There is a bounded Lipschitz constant L , which does not depend on the specific problem instance ($L = 25$ safely works for our reduction), such that either there exists Θ such that the function $f(\cdot, \Theta)$ is Lipschitz continuous with Lipschitz constant L and fits the data points, or there is no Θ at all to fit the data points. Using scaling on the labels, we can make the Lipschitz constant arbitrarily small. Note that Lipschitz continuity is also related to overfitting and regularization [41]. Recall that the purpose of regularization is to prefer simpler functions over more complicated ones. Being Lipschitz continuous with a small Lipschitz constant essentially means that the function is pretty flat. It is particularly remarkable that we can show hardness even for small Lipschitz constants since Lipschitz continuity has been a crucial assumption in several recent results about training *and* learning ReLU networks, for example, [11, 19, 36].

Simplicity. We consider it one of the strengths of our reduction that it is relatively simple and could be taught as part of a master’s-level course in computational geometry, machine learning or complexity.

Other Architectures. While we consider fully connected two-layer networks as the most important case, we are also interested in $\exists\mathbb{R}$ -hardness results for other network architectures. Specifically, fully connected three-layer neural networks and convolutional neural networks are interesting. This would strengthen our result and show that $\exists\mathbb{R}$ -completeness is a phenomenon that is robust, in other words independent of a choice of a specific network type.

Required Precision of Computation. In practice, we are often willing to accept small additive errors when computing $f(\cdot, \Theta)$ and therefore also do not need Θ to be of high precision. In other words, rounding the weights and biases Θ to the first “few” digits after the comma may be sufficient.

This way of modelling the problem seemingly allows to place the neural network training problem in NP . Yet we are not aware of such a proof. Let us note that most $\exists\mathbb{R}$ -complete problems can be relaxed so that they can be placed in NP [31], but guessing the digits of the solution in binary is in no way a practical algorithm to solve these problems. While worst case complexity does not always predict practical performance correctly and is overly pessimistic, it historically proved robust in predicting algorithmic difficulty.

Bienstock, Muñoz, and Pokutta [11] show that, in principle, arbitrary neural network architectures can be trained to approximate optimality via linear programs with size linear in the size of the data set, but exponential in the architecture size. Let us emphasize that the result [11] does not imply a witness of small size. This result complements $\exists\mathbb{R}$ -hardness because these linear programs provide only approximate solutions. Our $\exists\mathbb{R}$ -hardness result suggests that the same cannot be achieved for exact solutions.

1.3 Existential Theory of the Reals

The complexity class $\exists\mathbb{R}$ (pronounced as ‘ER’) has gained a lot of interest in recent years. It is defined via its canonical complete problem ETR (short for *Existential Theory of the Reals*) and contains all problems that polynomial-time many-one reduce to it. In an ETR instance we are given an integer n and a sentence of the form

$$\exists X_1, \dots, X_n \in \mathbb{R} : \varphi(X_1, \dots, X_n),$$

where φ is a well-formed and quantifier-free formula consisting of polynomial equations and inequalities in the variables and the logical connectives $\{\wedge, \vee, \neg\}$. The goal is to decide whether this sentence is true. As an example consider the formula $\varphi(X, Y) := X^2 + Y^2 \leq 1 \wedge Y^2 \geq 2X^2 - 1$; among (infinitely many) other solutions, $\varphi(0, 0)$ evaluates to true, witnessing that this is a yes-instance of ETR. It is known that

$$\text{NP} \subseteq \exists\mathbb{R} \subseteq \text{PSPACE}.$$

Here the first inclusion follows because a SAT instance can trivially be written as an equivalent ETR instance. The second inclusion is highly non-trivial and was first proven by Canny in his seminal paper [16].

Note that the complexity of working with continuous numbers was studied in various contexts. To avoid confusion, let us make some remarks on the underlying machine model. The underlying machine model for $\exists\mathbb{R}$ (over which sentences need to be decided and where reductions are performed in) is the word RAM (or equivalently, a Turing machine) and not the real RAM [31] or the Blum-Shub-Smale model [14].

The complexity class $\exists\mathbb{R}$ gains its importance by numerous important algorithmic problems that have been shown to be complete for this class in recent years. The name $\exists\mathbb{R}$ was introduced by Schaefer in [69] who also pointed out that several NP -hardness reductions from the literature actually implied $\exists\mathbb{R}$ -hardness. For this reason, several important $\exists\mathbb{R}$ -completeness results were obtained before the need for a dedicated complexity class became apparent.

Common features of $\exists\mathbb{R}$ -complete problems are their continuous solution space and the nonlinear relations between their variables. Important $\exists\mathbb{R}$ -completeness results include the realizability of abstract order types [58, 78] and geometric linkages [70], as well as the recognition of geometric segment [52, 55], unit-disk [50, 56], and ray intersection graphs [17]. More results appeared in the graph drawing community [27, 30, 54, 71], regarding polytopes [26, 67], the study of Nash-equilibria [10, 12, 13, 33, 72], matrix factorization [20, 73, 76, 77], or continuous constraint satisfaction problems [57]. In computational geometry, we would like to mention the art gallery problem [2] and covering polygons with convex polygons [1].

1.4 Neural Networks

We refer to this survey [9] for an extensive discussion on the mathematics of deep learning.

Expressivity of ReLU Networks. So-called *universal approximation theorems* state that a single hidden layer (with arbitrary width) is already sufficient to approximate every continuous function on a bounded domain with arbitrary precision [21, 48]. However, deeper networks require much less neurons to reach the same expressive power, yielding a potential theoretical explanation of the dominance of deep networks in practice [7, 29, 42, 44, 53, 62, 65, 68, 79, 80, 83]. Other related work includes counting and bounding the number of linear regions [43, 59, 60, 64, 65, 74], classifying the set of functions *exactly* representable by different architectures [7, 23, 46, 47, 61, 86], or analyzing the memorization capacity of ReLU networks [82, 84, 85].

Convergence of Gradient Descent. While (stochastic) gradient descent can easily get stuck in local minima, it still performs incredibly well in practical applications. A possible theoretical explanation for this behavior is that modern architectures have a massive amount of parameters. It has been shown that overparameterized neural networks trained by gradient descent behave similar to linear kernel methods, the so-called *neural tangent kernel* [49]. In this case, one can indeed prove global convergence of gradient descent [5, 28]. Note that this aligns with our observation above that training becomes easier when the number of neurons exceeds the number of data points.

Learning Theory. The most popular model to formalize learnability of the generalization error is *probably approximately correct* (PAC) learnability [75, 81]. There, one usually assumes that the true mapping from input to output values belongs to some *concept class* and the samples are drawn independently and identically distributed from an unknown underlying distribution. The goal is to return, with a high probability (over the sampling of the training data), a *hypothesis* that performs well on new samples drawn from the same distribution. If such a hypothesis can be found in polynomial time (and, therefore, with polynomially many samples), then we say that the concept class is *efficiently PAC learnable*. If the returned hypothesis is itself also an element of the concept class, then we call the learning algorithm *proper*.

While empirical risk minimization and PAC learnability are two different questions, they are strongly intertwined. First of all, given some conditions on the concept class (in terms of VC-dimension or Rademacher complexity), an efficient empirical risk minimization algorithm is usually a proper PAC learner [75]. The other direction is less clear. Nevertheless, a proper PAC learner applied to the uniform distribution over the training set yields an efficient *randomized* algorithm for empirical risk minimization [75]. Thus, in some randomized sense, one can say that empirical risk minimization and proper PAC learning are equivalent.

As we outlined above, for the concept class of neural networks, empirical risk minimization is NP-hard. Strategies to circumvent hardness from the perspective of learning theory include allowing improper learners, restricting the type of weights allowed in a neural network, imposing assumptions on the underlying distribution, or using learning models that are different from PAC. A large variety of successes has been achieved in this direction for neural networks in recent years. For example, Chen, Klivans, and Meka [19] showed fixed-parameter tractability of learning a ReLU network under some assumptions including Gaussian data and Lipschitz continuity of the network. We refer to [8, 18, 25, 36, 39, 37] as a non-exhaustive list of other results about (non-)learnability of ReLU networks in different settings.

1.5 Key Ingredients

For $\exists\mathbb{R}$ -membership we use a similar proof technique as is usually used to prove NP -membership. That is, we describe a witness and a verification algorithm. The main difference to NP -membership is that the witness is allowed to be real valued and is verified in the real RAM model [31].

To show $\exists\mathbb{R}$ -hardness, we reduce from an intermediate problem, which we prove to be $\exists\mathbb{R}$ -complete using a general result about continuous constraint satisfaction problems [57]. A bit simplified, it states that we only need to be able to encode ternary addition constraints as well as *any* binary nonlinear constraint satisfying some mild regularity conditions. Our construction works for the nonlinear constraint $xy + x + y = 0$. Apart from some technical details, the three main ideas of the proof are concerned with encoding variables, addition, and nonlinear constraints.

Variables. A natural candidate for encoding variables are the weights and biases of the neural network. However, those did not prove to be suitable for our purposes. The main problem with using the parameters of the neural network as variables is that the same function can be computed by neural networks with many different combinations of these parameters. There seems to be no easy way to normalize this directly.

To circumvent this issue, we work with the functions representable by fully connected two-layer neural networks directly. We frequently make use of the geometry of these functions. For now, it is only important to understand that each hidden neuron encodes a continuous piecewise linear function with exactly two pieces, separated by a *breakline*. Therefore, if we have m middle neurons, the function computed by the whole neural network is a continuous piecewise linear function with at most m breaklines separating the pieces of the function.

First, let us consider a neural network with only one input and one output neuron. We place a series of data points as seen in Figure 4. If we consider the functions $f(\cdot, \Theta)$ computed by a neural network with only four hidden neurons which fit these data points exactly, we can prove that these functions are all very similar. In fact, they only differ in one degree of freedom, namely the slope of the part around point p . This slope in essence represents our variable.

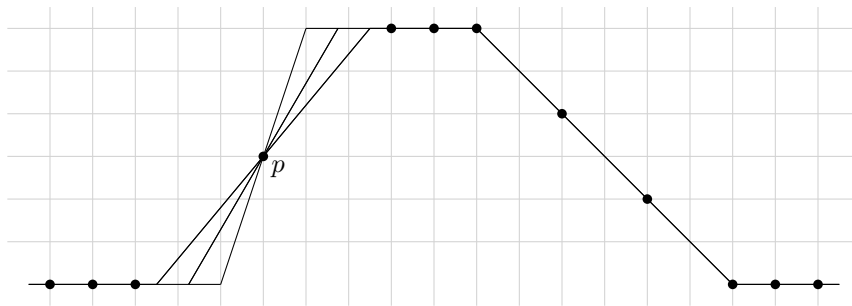


Figure 4: The slope around the data point p is flexible and can be used to encode a variable.

Addition. The key idea for encoding constraints between variables is that we can “read” the value of a variable using data points. At a point placed at a fixed location within the variable-encoding gadget, the function has a value which depends linearly on the value encoded by the gadget. To encode an addition constraint, we can therefore enforce the function to have a fixed value at a point lying in the intersection of multiple variable-encoding gadgets. This is simply achieved by placing a data point with a label depending on the desired value in this intersection.

To be able to intersect multiple variable-encoding gadgets, we need a second input dimension. Each variable-encoding gadget as seen in Figure 4 is now extended into a stripe in \mathbb{R}^2 , with Figure 4 showing only an orthogonal cross section of this stripe. Much of the technical difficulties lie in the subtleties to enforce the presence of multiple (possibly intersecting) gadgets in \mathbb{R}^2 using a finite number of data points.

For our reduction we need to be able to encode addition of three variables. Even in \mathbb{R}^2 , three lines (or stripes) are not guaranteed to intersect in a single point. We therefore make use of the capability to *copy* the value of one variable encoding gadget to another, using only binary addition.

Nonlinear Constraint. Within only a single output dimension, we are not able to encode nonlinear constraints [7]. We therefore add a second output dimension, which implies that the neural network represents two functions $f^1(\cdot, \Theta)$ and $f^2(\cdot, \Theta)$. Consequently, we are allowed to use data points with two different output labels, one for each output dimension.

One important observation is that the location of all of the breaklines of f only depend on the weights and biases in the first layer of the neural network. Thus, every breakline is present in both functions f^1 and f^2 , except if the corresponding weight to the output neuron is zero. This fact connects the two output dimensions in a way that we can utilize to encode our nonlinear constraints.

We define a nonlinearity gadget, which in \mathbb{R}^2 also corresponds to a stripe. For simplicity, we again introduce it only by showing a cross section. See Figure 5 for an illustration of this cross-section. In each single output dimension, the nonlinearity gadget looks exactly the same as the variable-encoding gadget. The nonlinearity gadget therefore carries *two* values.

One can prove that with only five breakpoints in total, the function can only fit all data points exactly if f^1 and f^2 share the breakpoint between p and q . This links the slopes of f^1 and f^2 in a nonlinear way, which enforces the nonlinear constraint between the variables encoded on this gadget.

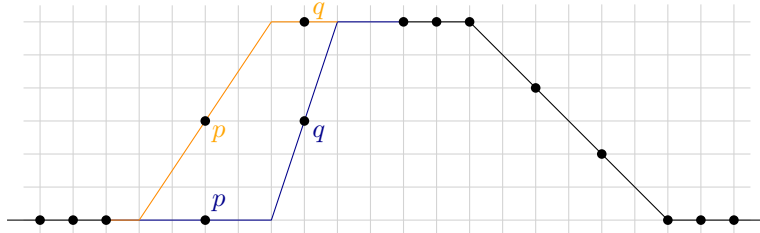


Figure 5: The function behaves differently in the two output dimensions. But as both output dimensions share the breakpoint between p and q , a nonlinear correspondence between the two slopes is enforced.

An additional technical challenge occurs when attempting to apply this nonlinear constraint to the values carried by two variable-encoding gadgets. As the nonlinearity gadget is fit differently in the two output dimensions, a data point enforcing equality between one of the values encoded on the nonlinearity gadget and the value encoded on a variable-encoding gadget needs to be “active” in only one output dimension. To achieve this, we also introduce a gadget which can be used to convert the label of a single data point p to an inequality $f(p, \Theta) \geq c$ in one or both output dimensions.

2 $\exists\mathbb{R}$ -Membership

Membership in $\exists\mathbb{R}$ is already proven in [3] by Abrahamsen, Kleist and Miltzow. In order to keep this paper self-contained while not being too repetitive, we shortly summarize their argument.

Applying a theorem from Erickson, Hoog and Miltzow [31], $\exists\mathbb{R}$ -membership can be shown by describing a polynomial-time *real verification algorithm*. Such an algorithm gets as input a TRAIN-F2NN instance I as well as a certificate Θ consisting of real-valued weights and biases. The instance I consists of a set D of data points, a network architecture and a target error γ . The algorithm then needs to verify that the neural network described by Θ fits all data points in D with a total error at most γ . The real verification algorithm is executed on a real RAM (see [31] for a formal definition). Thus, $\exists\mathbb{R}$ -membership can be shown just like NP-membership, the main difference being the underlying machine model (for NP-membership the verification algorithm must run on a word RAM instead).

A real verification algorithm for TRAIN-F2NN loops over all data points in D and evaluates the function described by the neural network for each of them. As in our case each hidden neuron uses ReLU as its activation function, each such evaluation takes linear time in the size of the network. The loss function can be computed in polynomial time on the real RAM (see also Definition 2 and the text afterwards).

3 A Hard Variant of ETR for Neural Networks

In this section we introduce ETR-NN, a restricted variant of ETR. An instance of ETR-NN is a conjunction of constraints that are tailored to our reduction in Section 4.

Recall that ETR is the decision problem whether a sentence of the form

$$\exists X_1, \dots, X_n \in \mathbb{R} : \varphi(X_1, \dots, X_n)$$

is true. Here φ is quantifier-free. Still, it can be an arbitrarily complicated logical formula of polynomial equations and inequalities. It is common practice in $\exists\mathbb{R}$ -completeness proofs to first reduce from ETR to a suitable variant that has a simpler logical structure and whose constraints can easily be encoded into gadgets. Miltzow and Schmiermann [57] gave two key conditions that are sufficient for $\exists\mathbb{R}$ -hardness: A ternary linear constraint and any binary nonlinear constraint. We formally show that ETR-NN satisfies these conditions.

Definition 4 (ETR-NN). Let φ be a quantifier-free formula with n free variables X_1, \dots, X_n that is a conjunction of constraints such that, for $X, Y, Z \in \{X_1, \dots, X_n\}$, each constraint is of exactly one of the four types

$$X + Y = Z, \quad XY + X + Y = 0, \quad X \geq 0, \quad \text{or} \quad X = 1.$$

We denote by ETR-NN the decision problem to decide sentences of the form

$$\exists X_1, \dots, X_n \in [-1, 1] : \varphi(X_1, \dots, X_n).$$

Lemma 5. ETR-NN is $\exists\mathbb{R}$ -complete.

Proof. We use a recent result of Miltzow and Schmiermann [57] (see Corollary 9 of the 3rd arXiv version). They provide two easy conditions that together imply $\exists\mathbb{R}$ -completeness of restricted variants of ETR. In particular, it is $\exists\mathbb{R}$ -complete to decide sentences of the form

$$\exists X_1, \dots, X_n \in [-1, 1] : \varphi(X_1, \dots, X_n),$$

where φ is a quantifier-free conjunction of constraints, each of exactly one of the four types

$$X + Y = Z, \quad g(X, Y) = 0, \quad X \geq 0, \quad X = 1,$$

for $X, Y, Z \in \{X_1, \dots, X_n\}$ and $g : [-1, 1]^2 \rightarrow \mathbb{R}$ being *well-behaved* and *curved around the origin* (both to be defined below). It remains to show that

$$\begin{aligned} g : [-1, 1]^2 &\rightarrow \mathbb{R} \\ (x, y) &\mapsto xy + x + y \end{aligned}$$

is well-behaved and curved around the origin. Following [57], function g is *well-behaved* if

- it is twice continuously differentiable on the interval $(-1, 1)^2$,
- $g(0, 0) = 0$ and all partial derivatives g_x, g_y, g_{xx}, g_{xy} and g_{yy} are rational at $(0, 0)$,
- $g_x(0, 0) \neq 0$ or $g_y(0, 0) \neq 0$, and
- $g(x, y)$ can be computed on a real RAM [31].

As g is a polynomial in $\mathbb{Z}[x, y]$ without constant part and since the coefficients of x and y are non-zero, it follows that the criteria above are satisfied.

For g to be *curved around the origin* we need to check that its curvature at $(0, 0)$ is non-zero. The curvature κ is defined as

$$\kappa(g) := \frac{g_y^2 g_{xx} - 2g_x g_y g_{xy} + g_x^2 g_{yy}}{(g_x^2 + g_y^2)^{3/2}},$$

whose denominator is always positive (because g is well-behaved). It is therefore sufficient to check that its numerator is non-zero at $(0, 0)$:

$$\begin{aligned} &(g_y^2 g_{xx} - 2g_x g_y g_{xy} + g_x^2 g_{yy})(0, 0) \\ &= ((x+1)^2 \cdot 0 - 2 \cdot (y+1) \cdot (x+1) \cdot 1 + (y+1)^2 \cdot 0)(0, 0) \\ &= (-2 \cdot (xy + y + x + 1))(0, 0) \\ &= -2 \end{aligned}$$

We conclude that the restricted variant from the statement is indeed $\exists\mathbb{R}$ -complete. \square

Let us remark that $\exists\mathbb{R}$ -completeness of ETR-NN is not too surprising. Consider $A = X - 1$ and $B = Y - 1$, then $XY + X + Y = 0$ becomes equivalent to $AB = 1$, which is just an inversion constraint. A similar ETR variant called ETR-INV (where inversion is the nonlinear binary constraint) was used for example in the $\exists\mathbb{R}$ -hardness reductions for the art gallery problem [2], drawing a graph in a polygonal region [54], drawing a graph with prescribed face areas [27], or training neural networks with not fully connected architectures [3].

4 $\exists\mathbb{R}$ -Hardness

In this section we present our $\exists\mathbb{R}$ -hardness reduction for TRAIN-F2NN. The reduction is mostly geometric, so we start by reviewing the underlying geometry of the two-layer neural networks considered in the paper in Section 4.1. This is followed by a high-level overview of the reduction in Section 4.2 before we describe the gadgets in detail in Section 4.3. Finally, in Section 4.4, we combine the gadgets into the proof of Theorem 3.

4.1 Geometry of Two-Layer Neural Networks

Our reduction below outputs a TRAIN-F2NN instance for a fully connected two-layer neural network N with two input neurons, two output neurons, and m hidden neurons. As defined above, for given weights and biases Θ , the network N realizes a function $f(\cdot, \Theta) : \mathbb{R}^2 \rightarrow \mathbb{R}^2$. The goal of this section is to build a geometric understanding of $f(\cdot, \Theta)$. We point the interested reader to these articles [7, 23, 46, 61, 86] investigating the set of functions exactly represented by different architectures of ReLU networks.

The i -th hidden ReLU neuron v_i realizes a function

$$\begin{aligned} f_i : \mathbb{R}^2 &\rightarrow \mathbb{R} \\ (x_1, x_2) &\mapsto \text{ReLU}(a_{1,i}x_1 + a_{2,i}x_2 + b_i), \end{aligned}$$

where $a_{1,i}, a_{2,i}$ are the edge weights from the first and second input neuron to v_i and b_i is its bias. We see that f_i is a continuous piecewise linear function: If $a_{1,i} = a_{2,i} = 0$, then $f_i = \max\{b_i, 0\}$ everywhere. Otherwise, the domain \mathbb{R}^2 is partitioned into two half-planes, touching along a so-called *breakline* given by the equation $a_{1,i}x_1 + a_{2,i}x_2 + b_i = 0$. The two half-planes are firstly the *inactive region* $\{(x_1, x_2) \subseteq \mathbb{R}^2 \mid a_{1,i}x_1 + a_{2,i}x_2 + b_i \leq 0\}$ in which f_i is constantly 0, and secondly the *active region* $\{(x_1, x_2) \subseteq \mathbb{R}^2 \mid a_{1,i}x_1 + a_{2,i}x_2 + b_i > 0\}$ in which f_i is positive and has a constant gradient, see Figure 6.

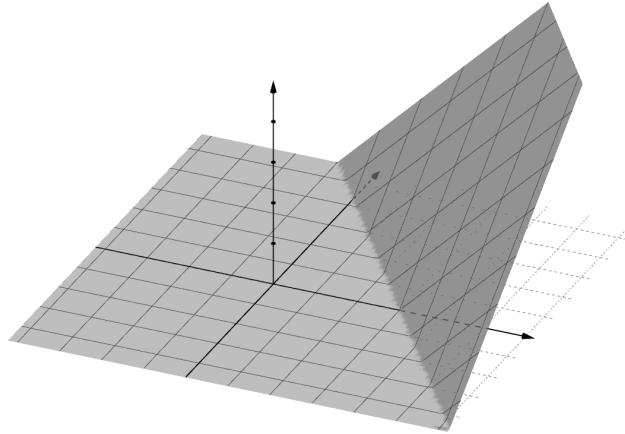


Figure 6: A continuous piecewise linear function computed by a hidden ReLU neuron. It has exactly one breakline; the left flat part is called the inactive region, whereas the right sloped part is the active region.

Now let $c_{i,1}, c_{i,2}$ be the weights of the edges connecting v_i with the first and second output neuron, respectively, and let $f(\cdot, \Theta) = (f^1(\cdot, \Theta), f^2(\cdot, \Theta))$. For $j \in \{1, 2\}$, the function $f^j(\cdot, \Theta) = \sum_{i=1}^m c_{i,j} \cdot f_i(\cdot, \Theta)$ is a weighted linear combination of the functions computed at the hidden neurons. We make three observations:

- As each function computed by a hidden ReLU neuron has at most one breakline, the domain of $f^j(\cdot, \Theta)$ is partitioned into the cells of a line arrangement of at most m *breaklines*. Inside each of these cells $f^j(\cdot, \Theta)$ has a constant gradient.
- The position of the breakline that a hidden neuron v_i contributes to $f^j(\cdot, \Theta)$ is determined solely by the $a_{\cdot,i}$ and b_i . In particular it is independent of $c_{i,j}$. Thus, the sets of breaklines partitioning $f^1(\cdot, \Theta)$ and $f^2(\cdot, \Theta)$ are both subsets of the same set: the set of (at most m) breaklines determined by the hidden neurons.

- Even if all m hidden neurons compute a function with a breakline, $f^j(\cdot, \Theta)$ might have less breaklines: It is possible for a breakline to be *erased* by setting $c_{i,j} = 0$, or for breaklines created by different hidden neurons to cancel each other out (producing no breakline) or lie on top of each other (combining multiple breaklines into one). In our reduction, we make use of $c_{i,j} = 0$ to erase some breaklines in a single output dimension, but we avoid the other two cases of breaklines combining/canceling.

In addition to these observations, note that, for each breakline, the change of the gradient of $f(\cdot, \Theta)$ when crossing the line is constant along the whole line. This allows to distinguish the following *types* of breaklines, which will ease our argumentation later.

Definition 6. A breakline ℓ is *concave* (*convex*) in $f^j(\cdot, \Theta)$, if the restriction of $f^j(\cdot, \Theta)$ to any two cells separated by ℓ in the breakline arrangement is concave (convex).

The *type* of a breakline is a tuple $(t_1, t_2) \in \{\wedge, 0, \vee\}^2$ describing whether the breakline is concave (\wedge), erased (0), or convex (\vee) in $f^1(\cdot, \Theta)$ and $f^2(\cdot, \Theta)$, respectively.

We have now established a basic geometric understanding of the function $f(\cdot, \Theta)$ computed by the neural network N . In our reduction we construct a data set which can be fit by a continuous piecewise linear function with m breaklines if and only if a given ETR-NN instance has a solution. To make sure that the continuous piecewise linear translates to a solution of the constructed TRAIN-F2NN instance, we need the following observation.

Observation 7. Let $f : \mathbb{R}^2 \rightarrow \mathbb{R}^2$ be a continuous piecewise linear function that can be described via a line arrangement \mathcal{L} of m lines with the following properties:

- In at least one cell of \mathcal{L} the value of f is constantly $(0, 0)$.
- For each line $\ell \in \mathcal{L}$ the change of the gradient of f when crossing ℓ is constant along ℓ .

Then there is a fully connected two-layer neural network with m hidden neurons computing f .

To see that this observation is true, consider the following construction. For each breakline add a hidden neuron realizing the breakline with the inactive region towards the constant- $(0, 0)$ cell, and with the correct change of gradients in each output dimension. It is easy to see that the sum of all these neurons computes f .

4.2 Reduction Overview

We show $\exists\mathbb{R}$ -hardness of TRAIN-F2NN (Definition 2) by giving a polynomial-time reduction from ETR-NN to TRAIN-F2NN. The reduction starts with an ETR-NN instance Φ and outputs an integer m and a set of n data points such that there is a fully connected two-layer neural network N with m hidden neurons exactly fitting all data points ($\gamma = 0$) if and only if Φ is true. Recall that for fixed weights and biases Θ the neural network N defines a continuous piecewise linear function $f(\cdot, \Theta) : \mathbb{R}^2 \rightarrow \mathbb{R}^2$.

For the reduction we define several *gadgets* representing parts (variables, linear and nonlinear constraints) of the ETR-NN instance Φ . Strictly speaking, a gadget is defined by a set of data points that need to be fit exactly. These data points serve two tasks: Firstly, most of the data points are used to enforce that $f(\cdot, \Theta)$ has m breaklines with predefined orientations and at almost predefined positions. Secondly, the remaining data points enforce relationships between the exact positions of different breaklines.

Globally, our construction yields $f(x, \Theta) = (0, 0)$ for “most” $x \in \mathbb{R}^2$. Each gadget consists of a constant number of parallel breaklines (enforced by data points) that lie in a *stripe* of constant

width in \mathbb{R}^2 . Only within these stripes $f(\cdot, \Theta)$ possibly attains non-zero values. Where two or more of these stripes intersect, additional data points can encode relations between the gadgets. The semantic meaning of a gadget is fully determined by the distances between its parallel breaklines. Thus each gadget can be translated and rotated arbitrarily without affecting its meaning.

Simplifications. Describing all gadgets purely by their data points is tedious and obscures the relatively simple geometry enforced by these data points. We therefore introduce two additional constructs, namely *data lines* and *weak data points*, that simplify the presentation. In particular, data lines impose breaklines, which in turn are needed to define gadgets. Weak data points are there to ensure that the gadgets used in the reduction encode variables with bounded range and that we can have features that are only active in one output dimension. How these constructs can be realized with carefully placed data points is deferred to Sections 4.3.5 and 4.3.6.

- A data line $(\ell; y)$ consists of a line $\ell \subseteq \mathbb{R}^2$ and a label giving the ground truth value $y \in \mathbb{R}^2$. When describing a single gadget, we want that all points $p \in \ell$ are exactly fit, that is, $f(p, \Theta) = y$. As soon as we consider several gadgets, their corresponding stripes in the domain \mathbb{R}^2 might intersect and we do not require that the data lines are fit correctly inside these intersections. As each data line will later be enforced by finitely many data points, we are able to choose coordinates for these defining data points that do not lie in any of these intersections.
- A weak data point relaxes a regular data point and prescribes only a lower bound on the value of the label. For example, we denote by $(x; y_1, \geq y_2)$ that $f^1(x, \Theta) = y_1$, and $f^2(x, \Theta) \geq y_2$. Weak data points can have such an inequality label in the first, the second, or both output dimensions.

Global Arrangement of Gadgets. We describe the global arrangement of the stripes belonging to all the gadgets in Section 4.4. However, in Figure 7 we already provide a rough picture to be kept in mind while we define all the gadgets individually.

4.3 Gadgets and Constraints

We describe all gadgets in isolation first and consider the interaction of two or more gadgets only where it is necessary. In particular, we assume that $f(x, \Theta)$ is constantly zero for $x \in \mathbb{R}^2$ outside of the outermost breaklines enforced by each gadget. After all gadgets have been introduced, we describe the global arrangement of the gadgets in Section 4.4. Recall that, since each gadget can be freely translated and rotated, we can describe the positions of all its data lines and (weak) data points relative to each other.

Not all gadgets make use of the two output dimensions. Some gadgets give the same labels in both output dimensions for all of their data lines, and thus look the same in both output dimensions. For these gadgets we simplify the usual notation of $(y_1, y_2) \in \mathbb{R}^2$ for labels to single-valued labels $y \in \mathbb{R}$. In our figures, data points and functions which look the same in both output dimensions are drawn in black, while features only occurring in one dimension are drawn in orange and blue to distinguish the dimensions from each other.

Let ℓ_1, \dots, ℓ_k be parallel data lines describing (parts of) a gadget. In an orthogonal cross section through the gadget, they are projected to points $p_i = (x_i, y_i)$, where x_i is the distance from ℓ_1 to ℓ_i and y_i is the label of ℓ_i .

Observation 8. *For a single output dimension, whenever three consecutive points p_i, p_{i+1}, p_{i+2} are not collinear in the cross section, then there must be a breakpoint (the intersection of a breakline b*

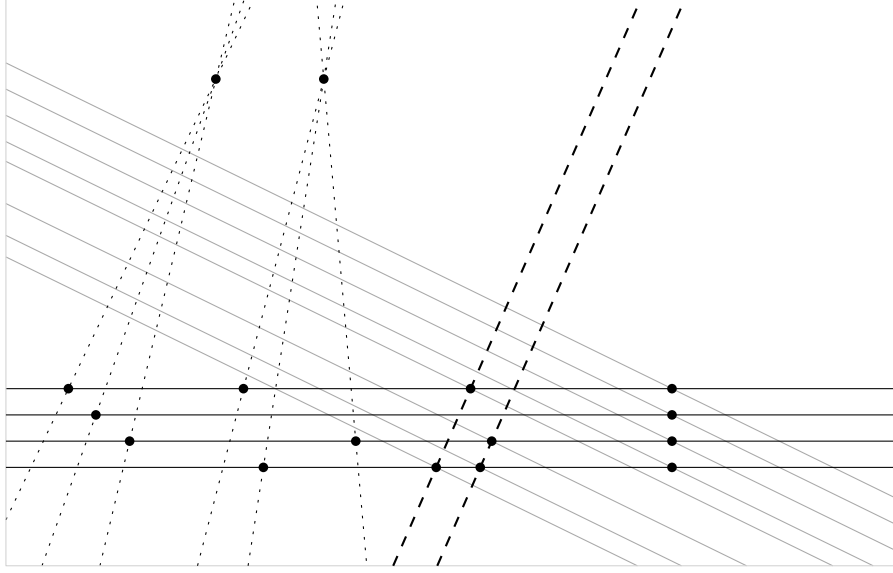


Figure 7: The overall layout of the arrangement of gadgets. The stripes in which the gadgets are defined are simplified to lines for clarity. Our construction contains the following types of gadgets: *variable gadgets* (solid, horizontal) representing a value for each variable in the ETR instance, more *variable gadgets* (dotted) copying these values and realizing linear constraints at intersections, *nonlinearity gadgets* (dashed) enforcing that two variables fulfill the nonlinear constraint of the ETR-NN instance, and so-called *cancel gadgets* (gray), which we use to realize weak data points.

with the cross section) strictly between p_i and p_{i+2} . Further, if p_{i+2} is above the line through p_i and p_{i+1} , b must be convex (\vee) in this output dimension. If otherwise p_{i+2} is below that line, b must be concave (\wedge) in this output dimension.

Observation 9. Whenever three consecutive points p_1, p_{i+1}, p_{i+2} are collinear in one of the two output dimensions, then there is either no breakpoint (active in this dimension) strictly between p_i and p_{i+2} , or at least two.

These observations are illustrated in Figure 8. Note that both observations not only hold if the cross section is orthogonal to the data lines but also at different angles.

In the analysis of each gadget, we use these observations to prove that the data lines enforce breaklines of a certain type with a prescribed orientation and (almost) fixed position.

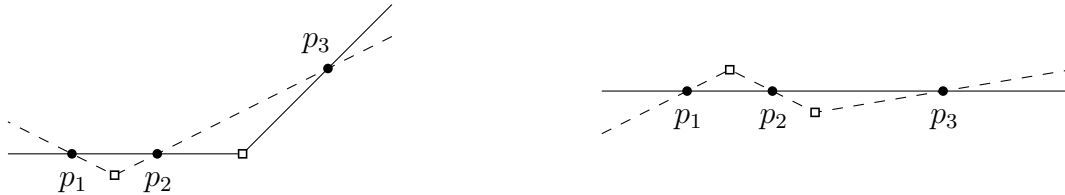


Figure 8: Three consecutive points in a cross section and possible interpolations with functions $f^j(\cdot, \Theta)$ in one of the two dimensions $j \in \{1, 2\}$. If the points are not collinear, then we need a breakpoint of a certain type, here convex (left). If the points are collinear, then there is either no breakpoint or there are at least two (right).

4.3.1 Variable Gadget

Recall that the values of all variables in ETR-NN are in the range $[-1, 1]$ by definition. In TRAIN-F2NN, values are encoded via a gadget that we call a *levee*, named after the shape $f(\cdot, \Theta)$ takes in each output dimension. As mentioned previously, the gadget only affects a stripe of bounded width. See Figure 9 for a cross section view through this stripe.

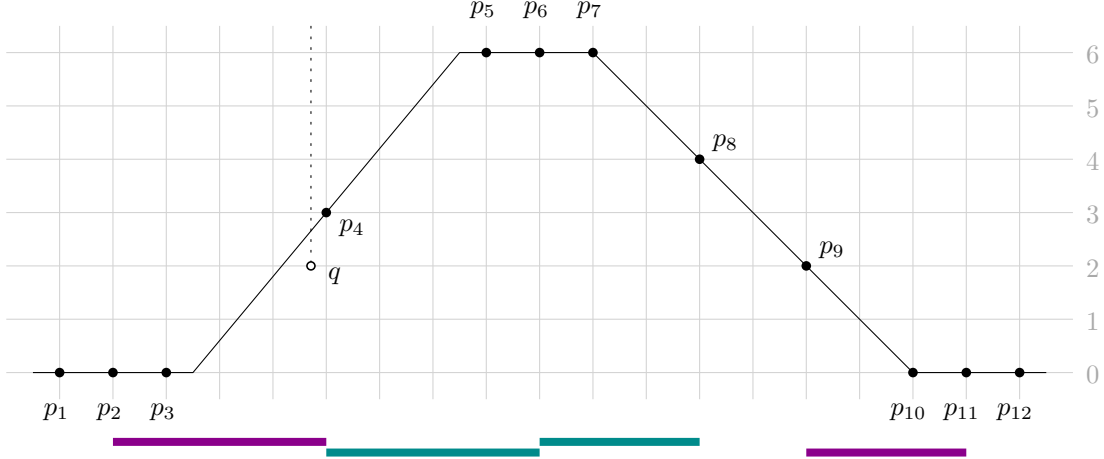


Figure 9: Orthogonal cross section view of a levee. The black points p_i are the projections of the data lines ℓ_1, \dots, ℓ_{12} , the white point q is a weak data point imposing a lower bound on $f(q, \Theta)$. The turquoise and purple bars below the cross section indicate non-collinear triples, where concave and convex breakpoints, respectively, are needed. For example, there needs to be a convex breakpoint in-between p_2 and p_4 .

A levee consists of four parallel breaklines b_1, b_2, b_3, b_4 , numbered from left to right. Left of b_1 and right of b_4 the value of $f(\cdot, \Theta)$ is constantly 0. Between b_2 and b_3 the value of $f(\cdot, \Theta)$ is constantly 6. The gradient of $f(\cdot, \Theta)$ between b_1 and b_2 is orthogonal to the breaklines and oriented towards b_2 . We call the Euclidean norm of the gradient between b_1 and b_2 the *slope* of the levee. The slope is always positive, so to realize values in the interval $[-1, 1]$, we say that a slope s_X encodes the value $X := s_X - 2$ and we will ensure the slope to be in the interval $[1, 3]$. This makes sure that values are in the interval $[-1, 1]$, as desired.

The gradient between b_3 and b_4 carries no semantic meaning. It is merely used to bring $f(\cdot, \Theta)$ back to 0, such that only a stripe in \mathbb{R}^2 is affected by the gadget. This part is thus fixed to a slope of 1 for simplicity.

We realize a levee using twelve parallel data lines, as described in the following table:

	ℓ_1	ℓ_2	ℓ_3	ℓ_4	ℓ_5	ℓ_6	ℓ_7	ℓ_8	ℓ_9	ℓ_{10}	ℓ_{11}	ℓ_{12}
distance to ℓ_1	0	1	2	5	8	9	10	12	14	16	17	18
label	0	0	0	3	6	6	6	4	2	0	0	0

Lemma 10. *Assume that at most four breaklines may be used. Then the twelve parallel data lines ℓ_1, \dots, ℓ_{12} as described in the table above realize a levee carrying a value in $[-1, \infty)$.*

Proof. We first prove that four breaklines are necessary to fit all data lines exactly. For this, consider an orthogonal cross section through the data lines. It is easy to see that the levee has four non-collinear triples (see Figure 9) and that they pairwise share at most one point. Thus, by Observation 8, four breaklines b_1, b_2, b_3, b_4 are indeed required.

As p_1, p_2, p_3 are collinear, we can further conclude by Observation 9 that b_1 has to intersect the cross section at p_3 or strictly between p_3 and p_4 . Similarly, as p_5, p_6, p_7 are collinear, we get that b_2 has to intersect the cross section at p_5 or strictly between p_4 and p_5 . The remaining breaklines b_3 and b_4 are fixed to intersect the cross section on p_7 and p_{10} , respectively.

Since this holds at every orthogonal cross section through the data lines, we further conclude that the breaklines are parallel to each other and to the data lines.

The exact positions of b_1 and b_2 depend on each other. As $f(\cdot, \Theta)$ must fit ℓ_4 , the distance between ℓ_4 and b_1 equals the distance between ℓ_4 and b_2 .

If $b_1 = \ell_3$ and $b_2 = \ell_5$, the slope of $f(\cdot, \Theta)$ between b_1 and b_2 is exactly 1. This is the minimum possible slope, because ℓ_3 and ℓ_5 have to be fit. There is no restriction on the maximum possible slope. Thus ℓ_1, \dots, ℓ_{12} realize a levee carrying a value in $[-1, \infty)$. \square

It remains to bound the value of the variable also from above, such that it is constrained to the interval $[-1, 1]$. To achieve this, we use a weak data point, named q in Figure 9. Recall that the label of a weak data point is a lower bound, and not a constant number.

Lemma 11. *Let q be a weak data point at distance $4\frac{2}{3}$ to ℓ_1 (and thus a distance of $\frac{1}{3}$ to ℓ_4) with lower bound label ≥ 2 . Then the slope of the levee is at most 3.*

Proof. Assume that the slope of $f(\cdot, \Theta)$ between b_1 and b_2 is strictly larger than 3. Then the contribution of the levee to $f(q, \Theta)$ is strictly less than 2, so the lower bound label of q is not satisfied. \square

We conclude that with twelve data lines and one weak data point we can enforce four parallel breaklines forming a levee, with a minimum slope of 1 and a maximum slope of 3, thus encoding a value in the interval $[-1, 1]$.

If the encoded ETR-NN instance has a constraint $X \geq 0$ for some variable X , then the levee corresponding to X is slightly modified: Data line ℓ_3 is moved further away from ℓ_1 and ℓ_2 by 1.5 such that the relative distance between ℓ_1 and ℓ_3 is increased to 3.5. Then the minimum possible slope for the levee is 2, thus representing a minimum value of 0.

4.3.2 Measuring a Value from a Levee

A levee represents a value to be used in the constraints. For every particular levee we consider the two parallel lines with distance 1 to ℓ_4 to be its *measuring lines*. We distinguish the *lower measuring line* (the one towards ℓ_3) and the *upper measuring line* (the one towards ℓ_5). Note that, since the slope of the levee is restricted to be in the interval $[1, 3]$, both measuring lines are always inside or at the boundary of the sloped part (in other words between breaklines b_1 and b_2).

Let s_X be the slope of the levee carrying X . At any point p on ℓ_4 , the contribution of the levee to $f(p, \Theta)$ is exactly 3, assuming ℓ_4 is fit exactly. From this it follows that for a point p_u on the upper measuring line the contribution to $f(p_u, \Theta)$ is $3 + s_X$. Thus, if we know the value of $f(p_u, \Theta)$ and further that p_u belongs to a single levee only, then we get $X = s_X - 2 = f(p_u, \Theta) - 5$ for the value represented by the levee. Similarly, for a point p_l on the lower measuring line the contribution to $f(p_l, \Theta)$ is $3 - s_X$. If p_l belongs to a single levee only, then $X = s_X - 2 = 1 - f(p_l, \Theta)$ is the represented value.

Figure 10 shows a cross section of a levee and its measuring lines.

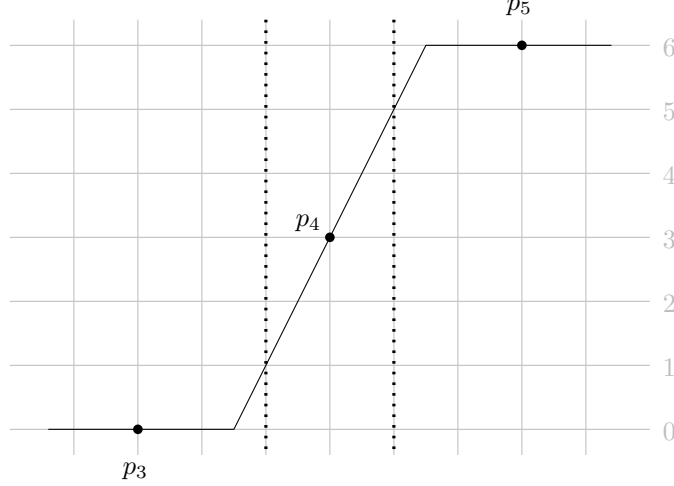


Figure 10: Partial cross section of a levee with slope s_X showing the lower and upper measuring lines (dotted). The contribution of this levee at these lines is $3 - s_X$ and $3 + s_X$, respectively. As can be seen, this levee has a slope of $s_X = 2$, thus encoding $X = 0$.

4.3.3 Enforcing Linear Constraints between Variables

For disjoint subsets \mathcal{A} and \mathcal{B} of the variables we can use an additional data point p to enforce a linear constraint of the form $\sum_{A \in \mathcal{A}} A = \sum_{B \in \mathcal{B}} B + c$. The value of the constant c can be chosen arbitrarily. Note that this type of constraint in particular allows us to make a variable gadget carry a constant value ($X = c$ via $\mathcal{A} = \{X\}, \mathcal{B} = \emptyset$), to make two variable gadgets carry the same value ($X = Y$ via $\mathcal{A} = \{X\}, \mathcal{B} = \{Y\}, c = 0$) or to encode a ternary addition ($X + Y = Z$ via $\mathcal{A} = \{X, Y\}, \mathcal{B} = \{Z\}, c = 0$).

The data point p is placed on a measuring line of each involved variable. For all variables in \mathcal{A} the data point p must be on the upper measuring line of the corresponding variable gadget. Similarly, for variables in \mathcal{B} the data point p must be on the lower measuring line. Therefore the levees of the involved variables need to be positioned such that the needed measuring lines all intersect at a common point, where p can be placed. This is trivial for $|\mathcal{A}| + |\mathcal{B}| \leq 2$, see Figure 11; but more involved for more variables, see Figure 12. Using the equality constraint $X = Y$, we can create copies of a variable on multiple levees, which can be positioned to obtain the required intersections. We discuss the global layout to achieve this in more detail in Section 4.4.

Lemma 12. *The constraint $\sum_{A \in \mathcal{A}} A = \sum_{B \in \mathcal{B}} B + c$ can be enforced by a data point p placed as described above with label $y = c + 5|\mathcal{A}| + |\mathcal{B}|$.*

Proof. First, let us consider a variable $A \in \mathcal{A}$ and let s_A be the slope of the corresponding levee. Data point p is placed on the upper measuring line of the levee, so it contributes $3 + s_A$ to $f(p, \Theta)$. Similarly, for a variable $B \in \mathcal{B}$ let s_B be the slope of its corresponding levee. Here p is placed on the lower measuring line and this levee contributes $3 - s_B$ to $f(p, \Theta)$.

The overall contribution of the levees of all involved variables adds up to

$$\begin{aligned} f(p, \Theta) &= \sum_{A \in \mathcal{A}} (3 + s_A) + \sum_{B \in \mathcal{B}} (3 - s_B) \\ &= \sum_{A \in \mathcal{A}} (5 + A) + \sum_{B \in \mathcal{B}} (1 - B), \end{aligned}$$

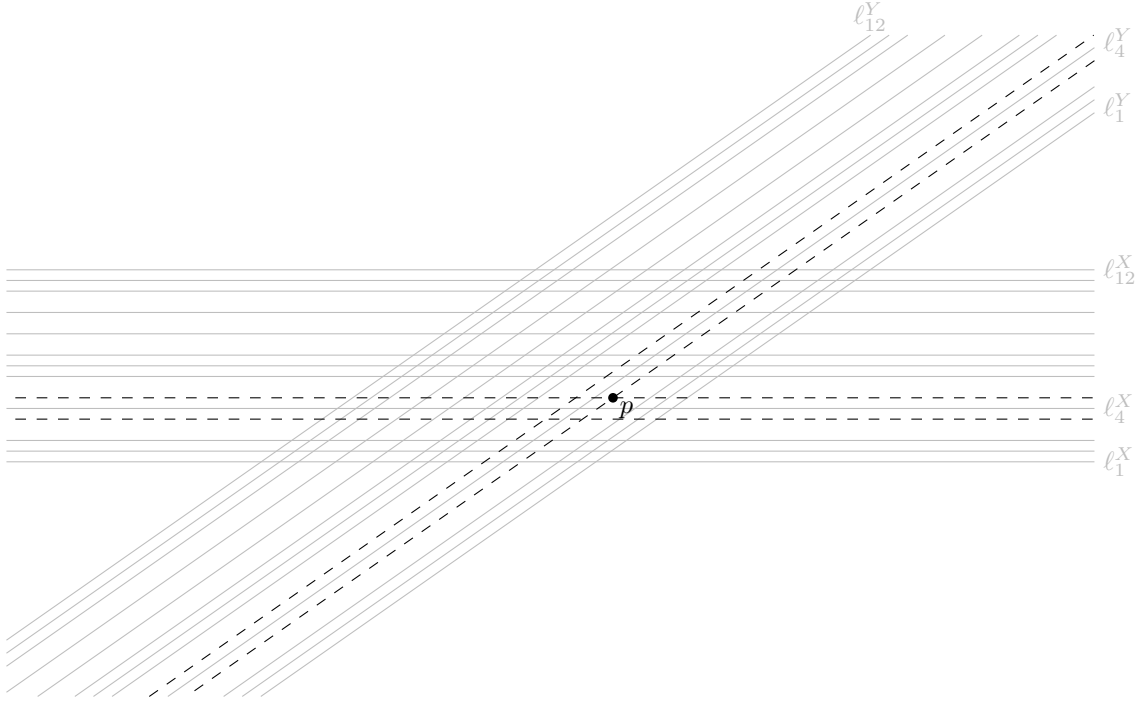


Figure 11: Top-down view on the intersection of two levees (gray) corresponding to two variables X and Y , and their measuring lines (black, dashed). The point p is placed at the intersection of the upper measuring line for X and lower measuring line for Y , and receives label 6 to enforce the constraint $X - Y = 0$.

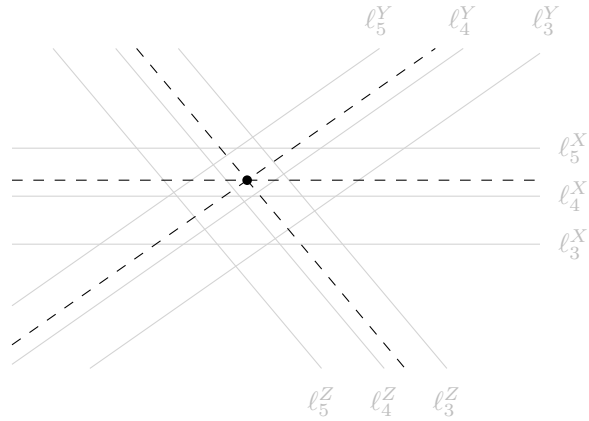


Figure 12: Top-down view of the interesting part of the intersection of three levees (gray) corresponding to variables X , Y , and Z , and their measuring lines (black, dashed). If the upper measuring lines for X and Y , as well as the lower measuring line for Z intersect at one point p , then imposing label 11 on p enforces a constraint of the form $X + Y = Z$.

where we used that the value represented by a levee is its slope minus 2. Choose the label of p to be $y = c + 5|\mathcal{A}| + |\mathcal{B}|$. Then, p is fit exactly if and only if the linear constraint $\sum_{A \in \mathcal{A}} A = \sum_{B \in \mathcal{B}} B + c$ is satisfied. \square

Lemma 12 is much more general than we actually require it for our reduction. An instance of ETR-NN can only have three different types of linear constraints. Surprisingly they can be encoded with data points using only two different labels:

Observation 13. *To encode the ternary addition constraint $X + Y = Z$ of ETR-NN the data point has label 11. For the constraints $X = 1$ and $X = Y$ the data point has label 6 in both cases.*

Until this point we did not distinguish between the two output dimensions of the levee. Let us note here that the data point enforcing the linear constraint can also be a weak data point, with a lower bound label of ≥ 0 in one of the output dimensions. As a levee has exactly the same breaklines (and therefore represents the same value) in both output dimensions, this is enough to enforce the constraint. We use this relaxation to realize nonlinear constraints in the following section.

4.3.4 Nonlinearity Gadget

We introduce a *nonlinearity gadget* which is in essence the superposition of two variable-encoding levees. This gadget uses data lines with different labels in the two output dimensions to enforce the presence of five parallel breaklines b_1, \dots, b_5 , instead of the usual four for a normal levee. In each output dimension, the continuous piecewise linear function defined by these five breaklines looks like a normal levee, that is, in each output dimension one of the breaklines is erased. The two levees share three breaklines, namely b_2, b_4 , and b_5 , where b_4 and b_5 form the constant-slope side of both levees. The breakline b_2 takes on different roles in the two levees – upper or lower breakline of the variable-slope side. The breaklines b_1 and b_3 take on the remaining role in one of the two levees, while being erased in the other output dimension, see Figure 13.

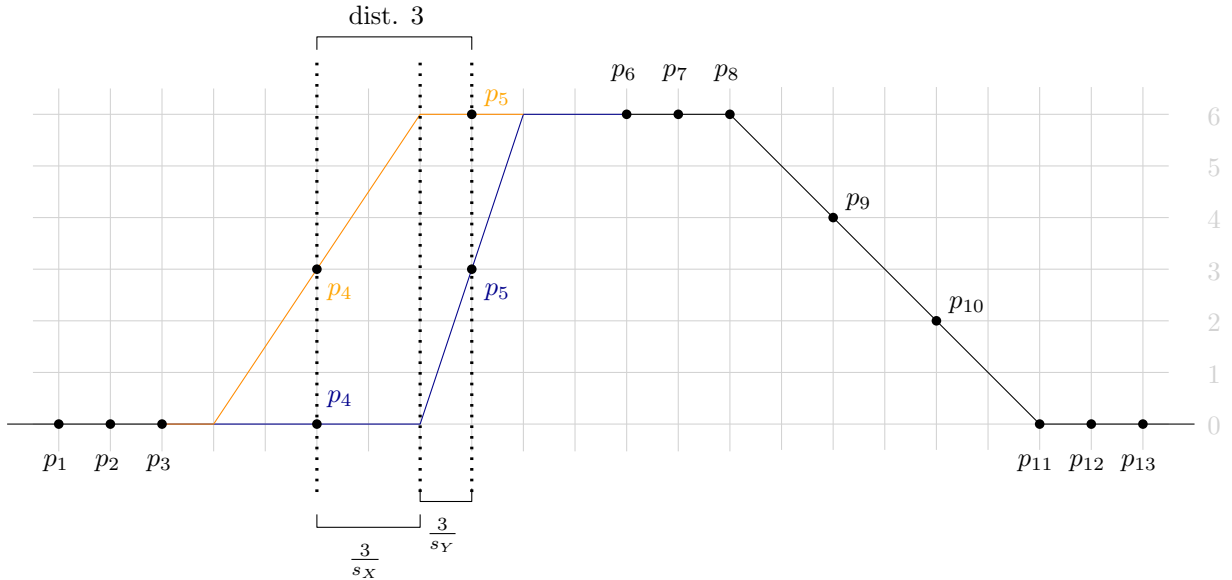


Figure 13: Cross section view of the nonlinearity gadget. The points p_1, \dots, p_{13} are the projections of the data lines ℓ_1, \dots, ℓ_{13} , where points p_4 and p_5 have different labels in the different output dimensions. Non-collinear triples of points force breaklines in-between them.

Analogous to a normal levee, a nonlinearity gadget carries two variables X, Y encoded by the slopes s_X and s_Y of the variable-slope side of the nonlinearity gadget in output dimension 1 and 2, respectively. Again, we have $X := s_X - 2$ and $Y := s_Y - 2$. The fact that the breakline b_2 is shared between the two levees enforces the desired nonlinear relationship $g(X, Y) = XY + X + Y = 0$ between the variables X, Y , as we will show below.

We define a nonlinearity gadget using 13 parallel data lines, positioned relatively to each other as follows:

	ℓ_1	ℓ_2	ℓ_3	ℓ_4	ℓ_5	ℓ_6	ℓ_7	ℓ_8	ℓ_9	ℓ_{10}	ℓ_{11}	ℓ_{12}	ℓ_{13}
distance to ℓ_1	0	1	2	5	8	11	12	13	15	17	19	20	21
label in dim. 1	0	0	0	3	6	6	6	6	4	2	0	0	0
label in dim. 2	0	0	0	0	3	6	6	6	4	2	0	0	0

Lemma 14. *Assume that at most five breaklines may be used. Then the 13 parallel data lines as described in the table above realize a nonlinearity gadget carrying two variables X, Y satisfying $XY + X + Y = 0$.*

Proof. First off, there must again be the two fixed breaklines b_4 and b_5 on the data lines ℓ_8 and ℓ_{11} , by the same arguments as for the normal levee.

There are four more relevant triples of non-collinear points, requiring the following breaklines:

- A breakline convex in output dimension 1 between ℓ_2 and ℓ_4 .
- A breakline convex in output dimension 2 between ℓ_3 and ℓ_5 .
- A breakline concave in output dimension 1 between ℓ_4 and ℓ_6 .
- A breakline concave in output dimension 2 between ℓ_5 and ℓ_7 .

Note that we need to fulfill all four of these requirements with only the three remaining breaklines. The first and the last requirement must be fulfilled by two different breaklines, as the intervals are disjoint. The breakline realizing the last requirement must be between ℓ_5 and ℓ_6 , as otherwise there would need to be at least one more breakline between ℓ_6 and ℓ_8 to fit the collinear points. Similarly, the breakline realizing the first requirement must be between ℓ_3 and ℓ_4 . Both of these breaklines must be inactive in one dimension, as otherwise the collinear points p_1, \dots, p_4 or p_5, \dots, p_8 , respectively, would not be fit properly. Thus, the remaining requirements must be fulfilled by the last available breakline, which must be concave in output dimension 1 and convex in output dimension 2, and between ℓ_4 and ℓ_5 .

As we now know the location and type of all breaklines, we can analyze the relationship between the variables carried on the two levees. The distance of ℓ_4 and ℓ_5 is 3. This distance can be subdivided into the distance from ℓ_4 to b_2 , and from b_2 to ℓ_5 . In the first part, $f^1(\cdot, \Theta)$ rises from 3 to 6, thus the distance must be $\frac{6-3}{s_X}$. For the second part, $f^2(\cdot, \Theta)$ rises from 0 to 3, and thus we can similarly say that the distance must be $\frac{3-0}{s_Y}$.

These distances must add up to 3, and thus the gadget encodes the constraint $\frac{3}{s_X} + \frac{3}{s_Y} = 3$, or equivalently $3s_Y + 3s_X = 3s_X s_Y$. In terms of variables, the constraint is therefore

$$3(Y + 2) + 3(X + 2) = 3(X + 2)(Y + 2) \iff XY + X + Y = 0,$$

which is our desired constraint. \square

To apply this constraint to two variables X and Y carried on two normal levees, we can build a nonlinearity gadget intersecting the levees of X and Y . In the intersection of the nonlinearity

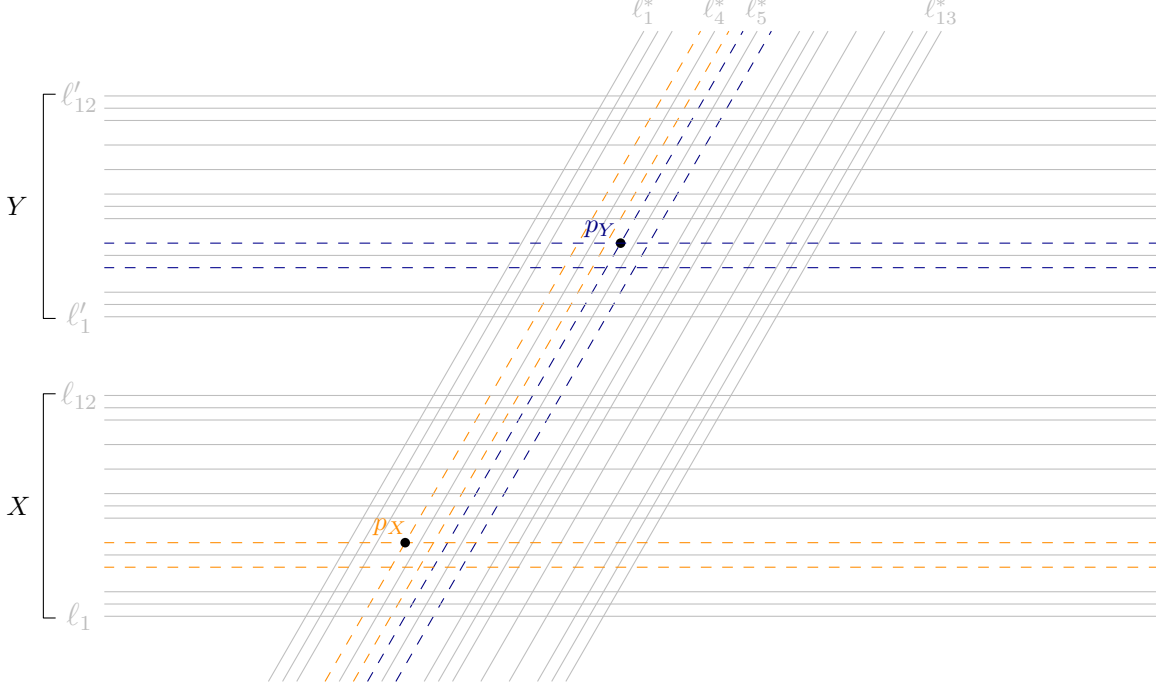


Figure 14: Top-down view on two levees (horizontal), denoted as X and Y ; their data lines (gray) and measuring lines (dashed). The sloped gadget is a nonlinearity gadget linking the two levees. Two weak data points (p_X and p_Y) are enforcing equality between the corresponding variables carried on the nonlinearity gadget and the normal levees.

gadget and the levee of X , we build a linear constraint enforcing the two variables to be equal, which is only “active” in the first output dimension. In the second output dimension the data point gets the trivially fulfilled label ≥ 0 . Similarly, at the intersection with the levee of Y , we build a linear constraint active only in the second output dimension and label ≥ 0 in the first output dimension. See Figure 14 for a top-down view on this construction.

As normal variable levees are the same in both output dimensions, this construction achieves that the constraint holding for the variables on the nonlinearity gadget now holds for the variables X and Y as well.

Note that the sloped parts of a nonlinearity gadget differ in the two output dimensions. In particular the measuring lines in dimension 1 have distance 1 to ℓ_4 , while the measuring lines in dimension 2 have distance 1 to ℓ_5 . Thus the data points enforcing equalities need to be placed on the measuring lines of the correct dimension.

We have now described all the needed gadgets with the help of data lines and weak data points. In the next two sections, we describe how those can be realized using only ordinary data points.

4.3.5 Realizing Weak Data Points

Recall that, for our construction so far, we used weak data points with labels of the form $\geq y$ in one or both output dimensions. We now introduce a gadget which can be used to realize such a weak data point using only non-weak data points (with constant labels). For each weak data point p we introduce a *cancel gadget*, consisting of three parallel breaklines that form a stripe containing p but no other (weak) data point.

A cancel gadget can be active in either one of the output dimensions, or in both of them. If a cancel gadget is active in some output dimension, the breaklines form a \vee shape of variable depth in that dimension. On the other hand, if the cancel gadget is inactive in some output dimension, the breaklines are all inactive (type 0) and the gadget contributes nothing to $f(\cdot, \Theta)$ in this dimension. The following table shows the locations and labels of the eight data lines that define a cancel gadget. The cancel gadget is illustrated in Figure 15.

	ℓ_1	ℓ_2	ℓ_3	ℓ_4	ℓ_5	ℓ_6	ℓ_7	ℓ_8
distance to ℓ_1	0	1	2	3	5	6	7	8
label in active dimension	0	0	0	-1	-1	0	0	0
label in inactive dimension	0	0	0	0	0	0	0	0

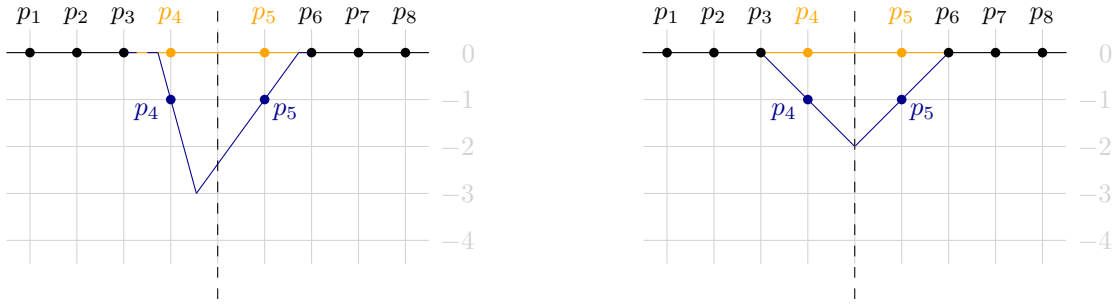


Figure 15: The cross section of a cancel gadget which is active in exactly one of the two output dimensions. It is used to “cancel” a weak data point in the active dimension (blue) that lies on the dashed vertical line. In the inactive dimension (orange) it does not contribute anything to $f(\cdot, \Theta)$, that is, all breaklines are erased (of type 0). The cancel gadget can be asymmetric (left), but it always has a maximum contribution to the weak data point of -2 (right).

Lemma 15. *Assume that at most three breaklines may be used. The eight data lines as described above realize a cancel gadget that contributes 0 to $f(p, \Theta)$ in an inactive dimension and an arbitrary amount $c \in (-\infty, -2]$ to $f(p, \Theta)$ in an active dimension to any point p with equal distance to ℓ_4 and ℓ_5 .*

Proof. Looking only at an active output dimension, there must be a concave breakline between ℓ_2 and ℓ_4 due to the non-collinear triple p_2, p_3, p_4 . Similarly, there must be a convex breakline between ℓ_3 and ℓ_5 , and between ℓ_4 and ℓ_6 . Lastly, there must again be a concave breakline between ℓ_5 and ℓ_7 . The two intervals requiring concave breaklines do not overlap, and we therefore need two concave breaklines. As there is only one breakline remaining, the two intervals requiring convex breaklines contain a single convex breakline in their intersection, that is, between ℓ_4 and ℓ_5 . The two concave breaklines must be between ℓ_3 and ℓ_4 (ℓ_5 and ℓ_6), as otherwise data line ℓ_3 (ℓ_6) is not properly fit.

To fit all data lines in the inactive output dimension, all breaklines must be inactive (type 0) in that dimension.

We can now analyze the possible contribution of the cancel gadget in an active output dimension to a point p equidistant to ℓ_4 and ℓ_5 . Any contribution $c \in (-\infty, -2]$ can be realized by placing breakline b_1 at distance $-1/(c+1)$ left of ℓ_4 , breakline b_3 at distance $-1/(c+1)$ right of ℓ_5 and breakline b_2 equidistant between ℓ_4 and ℓ_5 . A contribution $c > -2$ can not be realized, as otherwise there would need to be two convex breaklines, because p_3, p_4, p and p, p_5, p_6 are both non-collinear triples requiring a convex breakline. \square

Since the breaklines are at the exact same positions in both output dimensions we can observe the following:

Observation 16. *If the cancel gadget is active in both output dimensions, it contributes the same amount to the weak data point in both dimensions.*

The cancel gadget is placed such that the weak data point is equidistant to ℓ_4 and ℓ_5 . The inequality label $\geq y$ of the weak data point is converted to the constant label $y - 2$.

As shown above, the cancel gadget can contribute any value $c \in (-\infty, -2]$ to the data point. Thus, the data point can be fit perfectly if and only if the other gadgets contribute at least a value of y to the data point, that is, the intended weak constraint is met.

Lastly, let us note that a cancel gadget could also be constructed such that it has a \wedge shape and contributes a positive value in $[2, \infty)$ to the data point. This would allow constraints of the form $\leq y$ as well. Combining two cancel gadgets, one positive and one negative, would even allow a data point to attain an arbitrary value in \mathbb{R} (in one of the two dimensions), but this is not used in our reduction.

4.3.6 Realizing Data Lines using Data Points

We previously assumed that our gadgets are defined by data *lines*, but in the TRAIN-F2NN problem, we are only allowed to use data *points*. In this section, we argue that a set of data lines can be realized by replacing each data line by three data points. This in turn allows us to define the gadgets described throughout previous sections solely using data points.

Lemma 17. *Assume we are given a collection of gadgets as previously described which require a total of m breaklines. Then each data line can be replaced by three data points such that a continuous piecewise linear function with at most m breaklines fits the data points if and only if it fits the data lines.*

For the proof consider the line arrangement induced by the data lines. We introduce three vertical lines v_1, v_2, v_3 to the right of all intersections between the data lines. The vertical lines are placed at unit distance to one another. In our construction, no data line is vertical, thus each data line intersects each of the vertical lines exactly once. We place one data point on each intersection of each vertical line with a data line, inheriting the old label. Furthermore, on each vertical line, we ensure that the minimum distance α between any two data points belonging to different gadgets is larger than the maximum distance w between data points belonging to the same gadget. This can be achieved by placing the v_1, v_2 and v_3 far enough to the right and by ensuring a minimum distance between parallel gadgets.

Along each of the three vertical lines the data points form cross sections of all the gadgets, similar to the cross sections shown in Figures 9, 13 and 15. We have previously analyzed cross sections of individual gadgets in the proofs of Lemmas 10, 14 and 15. There we identified certain intervals bounded by data lines which each have to contain a *breakpoint* (the intersection of a breakline and the cross section). If we now consider the cross sections of all gadgets along the vertical lines, we refer to these intervals as *breakpoint intervals*. Note that a breakpoint interval sometimes consists of just one point. By the placement of the vertical lines, the cross sections (and thus also the breakpoint intervals) of different gadgets do not overlap.

Any two data lines bounding a breakpoint interval on v_1 also bound a breakpoint interval on v_2 and v_3 . We call the three breakpoint intervals on v_1, v_2 and v_3 which are bounded by the same data lines *matching* breakpoint intervals.

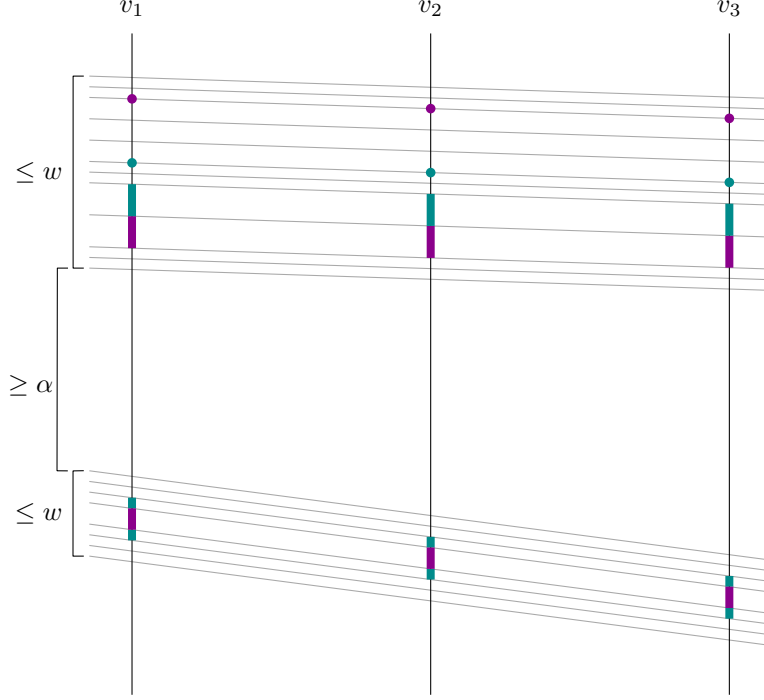


Figure 16: The data lines (gray) defining different gadgets (that is, a levee and a cancel gadget) and their intersections with the vertical lines v_1, v_2, v_3 . We add a data point at each intersection. The data points then enforce breaklines of different types in certain intervals (colored purple and turquoise). The values α and w describe the minimal distance between data lines of different gadgets, and the maximal distance between data lines of the same gadget, respectively.

In total there are $3m$ breakpoint intervals. We show that the only way to *stab* each of them exactly once using m breaklines is if each breakline stabs exactly three matching breakpoint intervals. The first observation towards this is that each breakline can only stab a single breakpoint interval per vertical line because all breakpoint intervals are pairwise disjoint. Thus, having m breakpoint intervals on each vertical line, each of the m breaklines has to stab exactly three intervals, one per vertical line. In a first step, we show that each breakline has to stab three breakpoint intervals belonging to the same gadget.

Claim 18. *Each breakline has to stab three breakpoint intervals of the same gadget.*

Proof. The proof is by induction on the number of gadgets. For a single gadget the claim trivially holds. For the inductive step, we consider the lowest gadget g (on v_1, v_2 and v_3) and assume for the sake of contradiction that there is a breakline b stabbing a breakpoint interval of g on v_2 and a breakpoint interval of a different gadget g' above g on v_1 . By construction, the minimum distance α between different gadgets is larger than the maximum width w of any gadget on all three vertical lines. Thus, the distance of any breakpoint interval of g' to any breakpoint interval of g on v_1 is larger than the width of g on v_3 . Therefore, we know that the breakline b intersects v_3 below any breakpoint intervals of g , which is the lowest gadget on v_3 . Thus it stabs at most two breakpoint intervals in total and therefore not all intervals can be stabbed. The same reasoning holds if the roles of v_1 and v_3 are flipped. All breaklines stabbing breakpoint intervals of g on v_2 must therefore also stab breakpoint intervals of g on v_1 and v_3 . Applying the induction hypothesis on the remaining gadgets, it follows that each breakline only stabs breakpoint intervals of the same gadget. \square

We can therefore analyze the situation for each gadget in isolation.

Claim 19. *To stab all $3 \cdot k$ breakpoint intervals required by a gadget with only k breaklines, each breakline has to stab three matching breakpoint intervals.*

The proof of this claim is straightforward but tedious and can be found in Appendix A. The main underlying idea is to use additional information about each breakpoint interval, namely the type of the required breakline. Breaklines must stab breakpoint intervals requiring the same type. From Claim 19, it also follows that within a single gadget, between the vertical lines no two breaklines can cross each other, nor can they cross a data line. Together with the previous claim, we can finally prove Lemma 17.

Proof of Lemma 17. By Claim 18 it follows that every breakline must stab three breakpoint intervals of the same gadget. By Claim 19 it follows then that each breakline must stab three matching breakpoint intervals, and therefore the breaklines do not cross any data lines between the three vertical lines.

It remains to show that the data points already ensure that each breakline b is parallel to the two parallel data lines d, d' enclosing it. To this end, consider the parallelogram defined by d, d', v_1, v_3 (see Figure 17) and let j be an output dimension in which b is active (not erased). Since no other breakline intersects this parallelogram, we obtain that f^j has exactly two linear pieces within the parallelogram, which are separated by b . Moreover, since b stabs matching breakpoint intervals, the three data points on d must belong to one of the pieces. Since these points have the same label, it follows that the gradient of this piece in output dimension j must be orthogonal to d (and, thus, to d' as well). Applying the same argument on the data points on d' , we obtain that the gradient of the other piece must be orthogonal to d and d' as well. This implies that also the difference of the gradients of the two pieces is orthogonal to d and d' . Finally, since b must be orthogonal to this difference of gradients, we obtain that it is parallel to d and d' . \square

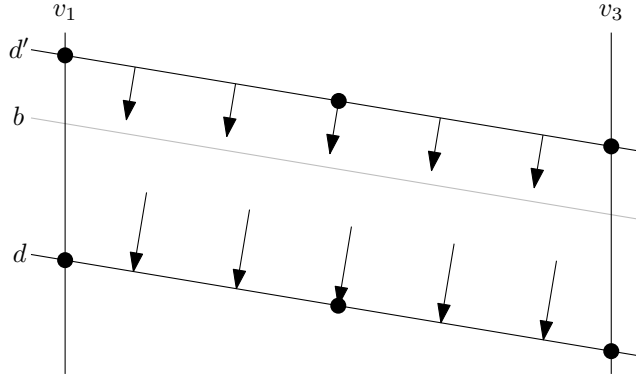


Figure 17: The parallelogram enclosed by the two data lines d, d' and the vertical lines v_1, v_3 . The three data points (black) on each data line enforce the gradient in both cells to be orthogonal to the data lines. As a consequence, the breakline b (gray) separating the cells has to be parallel to the data lines.

4.4 Global Construction Layout

We can now finalize proving $\exists\mathbb{R}$ -hardness of TRAIN-F2NN.

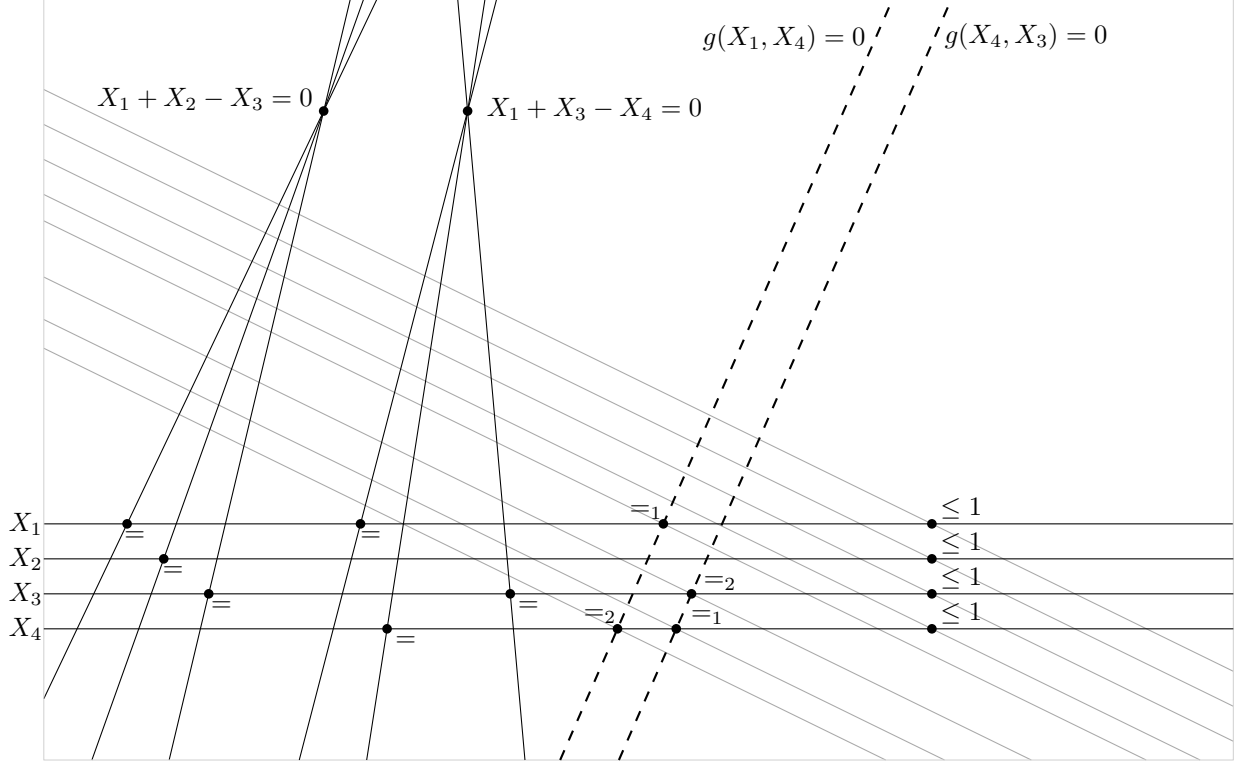


Figure 18: The layout of all gadgets and additional data points for the complete reduction. Each gadget is simplified to a single line for clarity. Black: levees. Dashed: nonlinearity gadgets. Gray: cancel gadgets. A point with label $=_i$ indicates an equality constraint only active in output dimension i .

For each variable X of the ETR-NN formula, we build a horizontal “canonical” levee carrying this variable at the bottom of the construction. As argued previously, the levees naturally ensure $X \geq -1$ for all variables X and the added weak data point with label ≥ 2 ensures $X \leq 1$. If the constraint $X \geq 0$ is present, the levee is built in the modified form enforcing this constraint (see Section 4.3.1).

All constraints of the form $X = 1$ are enforced using a linear constraint data point on the canonical levee carrying X .

The constraints of the form $X + Y = Z$ are enforced by copying all three involved variables onto a new levee using an equality constraint data point, with these three levees intersecting above all horizontal levees in a way such that the correct measuring lines of all three levees intersect in a single point. This allows a data point enforcing the constraint to be placed.

For the nonlinear constraints of the form $g(X, Y) = 0$ (let k be the number of such constraints), we build an array of k parallel nonlinearity gadgets intersecting all canonical levees. Each nonlinearity gadget is connected to the levees of the variables involved in the constraint by an equality constraint active in only one dimension.

Finally, we add a cancel gadget for each weak data point such that the cancel gadget contains only this data point but no other data points.

The complete layout can be seen in Figure 18, and an overview over all used gadgets and constructions can be seen in Table 1.

Table 1: An overview of all parts of the construction.

Gadget	#Breaklines	#Data Points	Labels
levee	4	37	$(0, 0), (2, 2), (3, 3), (4, 4), (6, 6)$
nonlinearity gadget	5	39	$(0, 0), (2, 2), (0, 3), (3, 6), (4, 4), (6, 6)$
linear link	0	1	$(11, 11), (-2, 6), (6, -2), (6, 6)$
cancel gadget	3	24	$(0, 0), (0, -1), (-1, 0), (-1, -1)$

Proof of Theorem 3. For $\exists\mathbb{R}$ -membership we refer to Section 2. For $\exists\mathbb{R}$ -hardness, we reduce ETR-NN, which is $\exists\mathbb{R}$ -complete by Lemma 5, to TRAIN-F2NN. Given an instance of ETR-NN, we construct an instance of TRAIN-F2NN with $\gamma = 0$ as previously described. Using all the lemmas we proved on the way, we obtain the following chain of equivalences, completing our reduction.

- The ETR-NN instance is a yes-instance.
- \Leftrightarrow There exists a satisfying assignment for the variables of the ETR-NN instance.
- \Leftrightarrow There exists a continuous piecewise linear function that fits all the data points of the TRAIN-F2NN instance and fulfills the conditions of Observation 7 with m breaklines.
- \Leftrightarrow There exists a fully connected two-layer neural network with m hidden ReLU neurons perfectly fitting all the data points.
- \Leftrightarrow The TRAIN-F2NN instance is a yes-instance.

The TRAIN-F2NN instance can be constructed in polynomial time, as the gadgets can be arranged in such a way that all data points (residing on intersections of lines) have coordinates which can be encoded in polynomial length.

The number of hidden neurons m is linear in the number of variables and the number of constraints of the ETR-NN instance. The number of data points can be bounded by $10 \cdot m$, thus the number of hidden neurons is linear in the number of data points.

As can be gathered from Table 1, the set of used labels is

$$\{(-2, 6), (-1, -1), (-1, 0), (0, -1), (0, 0), (0, 3), (2, 2), (3, 3), (3, 6), (4, 4), (6, -2), (6, 6), (11, 11)\}$$

with cardinality 13 as claimed. \square

Note that if the ETR-NN instance is satisfiable, each levee and nonlinearity gadget in a corresponding solution Θ to the constructed TRAIN-F2NN instance has a slope of at most 3 in each dimension. Furthermore, each cancel gadget must contribute at most 12 of negative value to satisfy its corresponding weak data point. Thus, there must also be a solution Θ' , where each cancel gadget is symmetric, and thus the function $f(\cdot, \Theta')$ is Lipschitz continuous with a low Lipschitz constant L , which in particular does not depend on the given ETR-NN instance. Checking all the different ways how our gadgets intersect, one can verify that $L = 25$ is sufficient.

References

- [1] Mikkel Abrahamsen. Covering Polygons is Even Harder. In Nisheeth K. Vishnoi, editor, *2021 IEEE 62nd Annual Symposium on Foundations of Computer Science (FOCS)*, pages 375–386, 2022. doi:[10.1109/FOCS52979.2021.00045](https://doi.org/10.1109/FOCS52979.2021.00045).
- [2] Mikkel Abrahamsen, Anna Adamaszek, and Tillmann Miltzow. The Art Gallery Problem is $\exists\mathbb{R}$ -complete. In *STOC 2018: Proceedings of the 50th Annual ACM SIGACT Symposium on Theory of Computing*, pages 65–73, 2018. doi:[10.1145/3188745.3188868](https://doi.org/10.1145/3188745.3188868).
- [3] Mikkel Abrahamsen, Linda Kleist, and Tillmann Miltzow. Training Neural Networks is ER-complete. In Marc A. Ranzato, Alina Beygelzimer, K. Nguyen, Percy Liang, Jennifer W. Vaughan, and Yann Dauphin, editors, *Advances in Neural Information Processing Systems (NeurIPS 2021)*, volume 34, 2021.
- [4] Mikkel Abrahamsen, Tillmann Miltzow, and Nadja Seifert. Framework for ER-Completeness of Two-Dimensional Packing Problems. In *2020 IEEE 61st Annual Symposium on Foundations of Computer Science (FOCS)*, pages 1014–1021, 2020. doi:[10.1109/FOCS46700.2020.00098](https://doi.org/10.1109/FOCS46700.2020.00098).
- [5] Zeyuan Allen-Zhu, Yuanzhi Li, and Zhao Song. A Convergence Theory for Deep Learning via Over-Parameterization. In Kamalika Chaudhuri and Ruslan Salakhutdinov, editors, *Proceedings of the 36th International Conference on Machine Learning (ICML 2019)*, volume 97 of *Proceedings of Machine Learning Research*, pages 242–252, 2019.
- [6] Alzinous. Fan Hui vs. AlphaGo - Game 5. <https://commons.wikimedia.org/wiki/File:FHvAG5.jpg>, 2016.
- [7] Raman Arora, Amitabh Basu, Poorya Mianjy, and Anirbit Mukherjee. Understanding Deep Neural Networks with Rectified Linear Units. In *International Conference on Learning Representations (ICLR 2018)*, 2018.
- [8] Ainesh Bakshi, Rajesh Jayaram, and David P. Woodruff. Learning Two Layer Rectified Neural Networks in Polynomial Time. In Alina Beygelzimer and Daniel Hsu, editors, *Proceedings of the Thirty-Second Conference on Learning Theory (COLT 2019)*, volume 99 of *Proceedings of Machine Learning Research*, pages 195–268, 2019.
- [9] Julius Berner, Philipp Grohs, Gitta Kutyniok, and Philipp Petersen. The Modern Mathematics of Deep Learning. arXiv preprint, 2021. arXiv:[2105.04026](https://arxiv.org/abs/2105.04026).
- [10] Marie L. T. Berthelsen and Kristoffer A. Hansen. On the Computational Complexity of Decision Problems About Multi-player Nash Equilibria. In Dimitris Fotakis and Evangelos Markakis, editors, *International Symposium on Algorithmic Game Theory*, volume 11801 of *Lecture Notes in Computer Science*, pages 153–167, 2019. doi:[10.1007/978-3-030-30473-7_11](https://doi.org/10.1007/978-3-030-30473-7_11).
- [11] Daniel Bienstock, Gonzalo Muñoz, and Sebastian Pokutta. Principled Deep Neural Network Training through Linear Programming. arXiv preprint, 2018. arXiv:[1810.03218](https://arxiv.org/abs/1810.03218).
- [12] Vittorio Bilò and Marios Mavronicolas. A Catalog of EXISTS-R-Complete Decision Problems About Nash Equilibria in Multi-Player Games. In Nicolas Ollinger and Heribert Vollmer, editors, *33rd Symposium on Theoretical Aspects of Computer Science (STACS 2016)*, Leibniz International Proceedings in Informatics (LIPIcs), pages 17:1–17:13, 2016. doi:[10.4230/LIPIcs.STACS.2016.17](https://doi.org/10.4230/LIPIcs.STACS.2016.17).

- [13] Vittorio Bilò and Marios Mavronicolas. Existential-R-Complete Decision Problems about Symmetric Nash Equilibria in Symmetric Multi-Player Games. In Vollmer Heribert and Brigitte Vallée, editors, *34th Symposium on Theoretical Aspects of Computer Science (STACS 2017)*, volume 66 of *Leibniz International Proceedings in Informatics (LIPIcs)*, pages 13:1–13:14, 2017. doi:[10.4230/LIPIcs.STACS.2017.13](https://doi.org/10.4230/LIPIcs.STACS.2017.13).
- [14] Lenore Blum, Mike Shub, and Steve Smale. On a Theory of Computation and Complexity over the Real Numbers: NP-Completeness, Recursive Functions and Universal Machines. *Bulletin of the American Mathematical Society*, 21:1–46, 1989. doi:[10.1090/S0273-0979-1989-15750-9](https://doi.org/10.1090/S0273-0979-1989-15750-9).
- [15] Digvijay Boob, Santanu S. Dey, and Guanghai Lan. Complexity of Training ReLU Neural Network. *Discrete Optimization*, 2020. in press. doi:[10.1016/j.disopt.2020.100620](https://doi.org/10.1016/j.disopt.2020.100620).
- [16] John Canny. Some Algebraic and Geometric Computations in PSPACE. In *STOC '88: Proceedings of the Twentieth Annual ACM Symposium on Theory of Computing*, pages 460–467, 1988. doi:[10.1145/62212.62257](https://doi.org/10.1145/62212.62257).
- [17] Jean Cardinal, Stefan Felsner, Tillmann Miltzow, Casey Tompkins, and Birgit Vogtenhuber. Intersection Graphs of Rays and Grounded Segments. *Journal of Graph Algorithms and Applications*, 22(2):273–294, 2018. doi:[10.7155/jgaa.00470](https://doi.org/10.7155/jgaa.00470).
- [18] Sitan Chen, Aravind Gollakota, Adam R. Klivans, and Raghu Meka. Hardness of Noise-Free Learning for Two-Hidden-Layer Neural Networks. arXiv preprint, 2022. arXiv:[2202.05258](https://arxiv.org/abs/2202.05258).
- [19] Sitan Chen, Adam R. Klivans, and Raghu Meka. Learning Deep ReLU Networks Is Fixed-Parameter Tractable. In Nisheeth K. Vishnoi, editor, *2021 IEEE 62nd Annual Symposium on Foundations of Computer Science (FOCS)*, pages 696–707, 2022. doi:[10.1109/FOCS52979.2021.00073](https://doi.org/10.1109/FOCS52979.2021.00073).
- [20] Dmitry Chistikov, Stefan Kiefer, Ines Marusic, Mahsa Shirmohammadi, and James Worrell. On Restricted Nonnegative Matrix Factorization. In Ioannis Chatzigiannakis, Michael Mitzenmacher, Yuval Rabani, and Davide Sangiorgi, editors, *43rd International Colloquium on Automata, Languages, and Programming (ICALP 2016)*, volume 55 of *Leibniz International Proceedings in Informatics (LIPIcs)*, pages 103:1–103:14, 2016. doi:[10.4230/LIPIcs.ICALP.2016.103](https://doi.org/10.4230/LIPIcs.ICALP.2016.103).
- [21] George Cybenko. Approximation by Superpositions of a Sigmoidal Function. *Mathematics of Control, Signals and Systems*, 2(4):303–314, 1989. doi:[10.1007/BF02551274](https://doi.org/10.1007/BF02551274).
- [22] Pedro J. de Rezende, Cid C. de Souza, Stephan Friedrichs, Michael Hemmer, Alexander Kröller, and Davi C. Tozoni. Engineering Art Galleries. In Lasse Kliemann and Peter Sanders, editors, *Algorithm Engineering: Selected Results and Surveys*, volume 9220 of *Lecture Notes in Computer Science*, pages 379–417. Springer, 1 edition, 2016. doi:[10.1007/978-3-319-49487-6](https://doi.org/10.1007/978-3-319-49487-6).
- [23] Steffen Dereich and Sebastian Kassing. On Minimal Representations of Shallow ReLU Networks. *Neural Networks*, 148:121–128, 2022. doi:[10.1016/j.neunet.2022.01.006](https://doi.org/10.1016/j.neunet.2022.01.006).
- [24] Santanu S. Dey, Guany Wang, and Yao Xie. Approximation Algorithms for Training One-Node ReLU Neural Networks. *IEEE Transactions on Signal Processing*, 68:6696–6706, 2020. doi:[10.1109/TSP.2020.3039360](https://doi.org/10.1109/TSP.2020.3039360).

- [25] Ilias Diakonikolas, Surbhi Goel, Sushrut Karmalkar, Adam R. Klivans, and Mahdi Soltanolkotabi. Approximation Schemes for ReLU Regression. In Jacob Abernethy and Shivani Agarwal, editors, *Proceedings of Thirty Third Conference on Learning Theory (COLT 2020)*, volume 125 of *Proceedings of Machine Learning Research*, pages 1452–1485, 2020.
- [26] Michael G. Dobbins, Andreas Holmsen, and Tillmann Miltzow. A Universality Theorem for Nested Polytopes. arXiv preprint, 2019. [arXiv:1908.02213](#).
- [27] Michael G. Dobbins, Linda Kleist, Tillmann Miltzow, and Paweł Rzażewski. $\forall\exists\mathbb{R}$ -Completeness and Area-Universality. In Andreas Brandstädt, Ekkehard Köhler, and Klaus Meer, editors, *Graph-Theoretic Concepts in Computer Science (WG 2018)*, volume 11159 of *Lecture Notes in Computer Science*, pages 164–175. Springer, 2018. [doi:10.1007/978-3-030-00256-5_14](#).
- [28] Simon Du, Jason Lee, Haochuan Li, Liwei Wang, and Xiyu Zhai. Gradient Descent Finds Global Minima of Deep Neural Networks. In Kamalika Chaudhuri and Ruslan Salakhutdinov, editors, *Proceedings of the 36th International Conference on Machine Learning (ICML 2019)*, volume 97 of *Proceedings of Machine Learning Research*, pages 1675–1685, 2019.
- [29] Ronen Eldan and Ohad Shamir. The Power of Depth for Feedforward Neural Networks. In Vitaly Feldman, Alexander Rakhlin, and Ohad Shamir, editors, *29th Annual Conference on Learning Theory (COLT 2016)*, volume 49 of *Proceedings of Machine Learning Research*, pages 907–940, 2016.
- [30] Jeff Erickson. Optimal Curve Straightening is $\exists\mathbb{R}$ -Complete. arXiv preprint, 2019. [arXiv:1908.09400](#).
- [31] Jeff Erickson, Ivor van der Hoog, and Tillmann Miltzow. Smoothing the gap between NP and ER. In *2020 IEEE 61st Annual Symposium on Foundations of Computer Science (FOCS)*, pages 1022–1033, 2020. [doi:10.1109/FOCS46700.2020.00099](#).
- [32] Vincent Froese, Christoph Hertrich, and Rolf Niedermeier. The Computational Complexity of ReLU Network Training Parameterized by Data Dimensionality. arXiv preprint, 2021. [arXiv:2105.08675](#).
- [33] Jugal Garg, Ruta Mehta, Vijay V. Vazirani, and Sadra Yazdanbod. $\exists\mathbb{R}$ -Completeness for Decision Versions of Multi-Player (Symmetric) Nash Equilibria. *ACM Transactions on Economics and Computation*, 6(1):1:1–1:23, 2018. [doi:10.1145/3175494](#).
- [34] Thierry Gensane and Philippe Ryckelynck. Improved Dense Packings of Congruent Squares in a Square. *Discrete & Computational Geometry*, 34(1):97–109, 2005. [doi:10.5555/3115441.3115583](#).
- [35] Xavier Glorot, Antoine Bordes, and Yoshua Bengio. Deep Sparse Rectifier Neural Networks. In Geoffrey Gordon, David Dunson, and Miroslav Dudík, editors, *Proceedings of the Fourteenth International Conference on Artificial Intelligence and Statistics (AISTATS 2011)*, volume 15 of *Proceedings of Machine Learning Research*, pages 315–323, 2011.
- [36] Surbhi Goel, Varun Kanade, Adam R. Klivans, and Justin Thaler. Reliably Learning the ReLU in Polynomial Time. In Satyen Kale and Ohad Shamir, editors, *Proceedings of the 2017 Conference on Learning Theory (COLT 2017)*, volume 65 of *Proceedings of Machine Learning Research*, pages 1004–1042, 2017.

- [37] Surbhi Goel and Adam R. Klivans. Learning Neural Networks with Two Nonlinear Layers in Polynomial Time. In Alina Beygelzimer and Daniel Hsu, editors, *Proceedings of the Thirty-Second Conference on Learning Theory (COLT 2019)*, volume 99 of *Proceedings of Machine Learning Research*, pages 1470–1499, 2019.
- [38] Surbhi Goel, Adam R. Klivans, Pasin Manurangsi, and Daniel Reichman. Tight Hardness Results for Training Depth-2 ReLU Networks. In James R. Lee, editor, *12th Innovations in Theoretical Computer Science Conference (ITCS 2021)*, volume 185 of *Leibniz International Proceedings in Informatics (LIPIcs)*, pages 22:1–22:14, 2021. doi:[10.4230/LIPIcs.ITCS.2021.22](https://doi.org/10.4230/LIPIcs.ITCS.2021.22).
- [39] Surbhi Goel, Adam R. Klivans, and Raghu Meka. Learning One Convolutional Layer with Overlapping Patches. In Jennifer Dy and Andreas Krause, editors, *Proceedings of the 35th International Conference on Machine Learning (ICML 2018)*, volume 80 of *Proceedings of Machine Learning Research*, pages 1783–1791, 2018.
- [40] Ian Goodfellow, Yoshua Bengio, and Aaron Courville. *Deep Learning*. MIT Press, 2016. <http://www.deeplearningbook.org>.
- [41] Henry Gouk, Eibe Frank, Bernhard Pfahringer, and Michael J. Cree. Regularisation of neural networks by enforcing Lipschitz continuity. *Machine Learning*, 110(2):393–416, 2021. doi:[10.1007/s10994-020-05929-w](https://doi.org/10.1007/s10994-020-05929-w).
- [42] Boris Hanin. Universal Function Approximation by Deep Neural Nets with Bounded Width and ReLU Activations. *Mathematics*, 7(10):992:1–9, 2019. doi:[10.3390/math7100992](https://doi.org/10.3390/math7100992).
- [43] Boris Hanin and David Rolnick. Complexity of Linear Regions in Deep Networks. In Kamalika Chaudhuri and Ruslan Salakhutdinov, editors, *Proceedings of the 36th International Conference on Machine Learning (ICML 2019)*, volume 97 of *Proceedings of Machine Learning Research*, pages 2596–260, 2019.
- [44] Boris Hanin and Mark Sellke. Approximating Continuous Functions by ReLU Nets of Minimal Width. arXiv preprint, 2018. arXiv:[1710.11278](https://arxiv.org/abs/1710.11278).
- [45] Simon B. Hengeveld and Tillmann Miltzow. A Practical Algorithm with Performance Guarantees for the Art Gallery Problem. In Kevin Buchin and Éric Colin de Verdière, editors, *37th International Symposium on Computational Geometry (SoCG 2021)*, volume 189 of *Leibniz International Proceedings in Informatics (LIPIcs)*, pages 44:1–44:16, 2021. doi:[10.4230/LIPIcs.SocG.2021.44](https://doi.org/10.4230/LIPIcs.SocG.2021.44).
- [46] Christoph Hertrich, Amitabh Basu, Marco Di Summa, and Martin Skutella. Towards Lower Bounds on the Depth of ReLU Neural Networks. In Marc A. Ranzato, Alina Beygelzimer, K. Nguyen, Percy Liang, Jennifer W. Vaughan, and Yann Dauphin, editors, *Advances in Neural Information Processing Systems (NeurIPS 2021)*, volume 34, 2021.
- [47] Christoph Hertrich and Leon Sering. ReLU Neural Networks of Polynomial Size for Exact Maximum Flow Computation. arXiv preprint, 2021. arXiv:[2102.06635](https://arxiv.org/abs/2102.06635).
- [48] Kurt Hornik. Approximation Capabilities of Multilayer Feedforward Networks. *Neural Networks*, 4(2):251–257, 1991. doi:[10.1016/0893-6080\(91\)90009-T](https://doi.org/10.1016/0893-6080(91)90009-T).
- [49] Arthur Jacot, Franck Gabriel, and Clément Hongler. Neural Tangent Kernel: Convergence and Generalization in Neural Networks. In Samy Bengio, Hanna Wallach, Hugo Larochelle, Kristen

- Grauman, Nicolò Cesa-Bianchi, and Roman Garnett, editors, *Advances in Neural Information Processing Systems (NeurIPS 2018)*, volume 31, 2018.
- [50] Ross Kang and Tobias Müller. Sphere and Dot Product Representations of Graphs. *Discrete & Computational Geometry*, 47(3):548–569, 2012. doi:[10.1007/s00454-012-9394-8](https://doi.org/10.1007/s00454-012-9394-8).
 - [51] Sammy Khalife and Amitabh Basu. Neural networks with linear threshold activations: structure and algorithms. In *International Conference on Integer Programming and Combinatorial Optimization (IPCO; to appear)*, 2022.
 - [52] Jan Kratochvíl and Jiří Matoušek. Intersection Graphs of Segments. *Journal of Combinatorial Theory, Series B*, 62(2):289–315, 1994. doi:[10.1006/jctb.1994.1071](https://doi.org/10.1006/jctb.1994.1071).
 - [53] Shiyu Liang and Rayadurgam Srikant. Why Deep Neural Networks for Function Approximation? In *International Conference on Learning Representations (ICLR 2017)*, 2017.
 - [54] Anna Lubiw, Tillmann Miltzow, and Debajyoti Mondal. The Complexity of Drawing a Graph in a Polygonal Region. In Therese Biedl and Andreas Kerren, editors, *GD 2018: Graph Drawing and Network Visualization*, volume 11282 of *Lecture Notes in Computer Science*, pages 387–401, 2018. doi:[10.1007/978-3-030-04414-5_28](https://doi.org/10.1007/978-3-030-04414-5_28).
 - [55] Jiří Matoušek. Intersection graphs of segments and $\exists\mathbb{R}$. arXiv preprint, 2014. arXiv:[1406.2636](https://arxiv.org/abs/1406.2636).
 - [56] Colin McDiarmid and Tobias Müller. Integer realizations of disk and segment graphs. *Journal of Combinatorial Theory, Series B*, 103(1):114–143, 2013. doi:[10.1016/j.jctb.2012.09.004](https://doi.org/10.1016/j.jctb.2012.09.004).
 - [57] Tillmann Miltzow and Reinier F. Schmiermann. On Classifying Continuous Constraint Satisfaction Problems. In Nisheeth K. Vishnoi, editor, *2021 IEEE 62nd Annual Symposium on Foundations of Computer Science (FOCS)*, pages 781–791, 2022. doi:[10.1109/FOCS52979.2021.00081](https://doi.org/10.1109/FOCS52979.2021.00081).
 - [58] Nikolai E. Mnëv. The Universality Theorems on the Classification Problem of Configuration Varieties and Convex Polytopes Varieties. In Oleg Y. Viro and Anatoly M Vershik, editors, *Topology and Geometry — Rohlin Seminar*, volume 1346 of *Lecture Notes in Mathematics*, pages 527–543. Springer, 1988. doi:[10.1007/BFb0082792](https://doi.org/10.1007/BFb0082792).
 - [59] Guido Montúfar, Yue Ren, and Leon Zhang. Sharp bounds for the number of regions of maxout networks and vertices of Minkowski sums. arXiv preprint, 2021. arXiv:[2104.08135](https://arxiv.org/abs/2104.08135).
 - [60] Guido F. Montúfar, Razvan Pascanu, Kyunghyun Cho, and Yoshua Bengio. On the Number of Linear Regions of Deep Neural Networks. In Zoubin Ghahramani, Max Welling, Corinna Cortes, Neil Lawrence, and Weinberger Kilian Q., editors, *Proceedings of the 27th International Conference on Neural Information Processing Systems (NeurIPS 2014)*, volume 2, pages 2924–2932, 2014.
 - [61] Anirbit Mukherjee and Amitabh Basu. Lower bounds over Boolean inputs for deep neural networks with ReLU gates. arXiv preprint, 2017. arXiv:[1711.03073](https://arxiv.org/abs/1711.03073).
 - [62] Quynh Nguyen, Mahesh Chandra Mukkamala, and Matthias Hein. Neural Networks Should Be Wide Enough to Learn Disconnected Decision Regions. In Jennifer Dy and Andreas Krause, editors, *Proceedings of the 35th International Conference on Machine Learning (ICML 2018)*, volume 80 of *Proceedings of Machine Learning Research*, pages 3740–3749, 2018.

- [63] Owlsmcgee. Image of a young woman generated by StyleGAN. https://commons.wikimedia.org/wiki/File:Woman_1.jpg, 2019.
- [64] Razvan Pascanu, Guido Montúfar, and Yoshua Bengio. On the number of response regions of deep feed forward networks with piece-wise linear activations. In *International Conference on Learning Representations (ICLR 2014)*, 2014.
- [65] Maithra Raghu, Ben Poole, Jon Kleinberg, Surya Ganguli, and Jascha Sohl-Dickstein. On the Expressive Power of Deep Neural Networks. In Doina Precup and Yee Whye Teh, editors, *Proceedings of the 34th International Conference on Machine Learning (ICML 2017)*, volume 70 of *Proceedings of Machine Learning Research*, pages 2847–2854, 2017.
- [66] Daniel Richardson. Some Undecidable Problems Involving Elementary Functions of a Real Variable. *The Journal of Symbolic Logic*, 33(4):514–520, 1969. doi:10.2307/2271358.
- [67] Jürgen Richter-Gebert and Günter M. Ziegler. Realization Spaces of 4-Polytopes are Universal. *Bulletin of the American Mathematical Society*, 32(4):403–412, 1995. doi:10.1090/S0273-0979-1995-00604-X.
- [68] Itay Safran and Ohad Shamir. Depth-Width Tradeoffs in Approximating Natural Functions with Neural Networks. In Doina Precup and Yee Whye Teh, editors, *Proceedings of the 34th International Conference on Machine Learning (ICML 2017)*, volume 70 of *Proceedings of Machine Learning Research*, pages 2979–2987, 2017.
- [69] Marcus Schaefer. Complexity of Some Geometric and Topological Problems. In David Eppstein and Emden R. Gansner, editors, *GD 2009: Graph Drawing*, volume 5849 of *Lecture Notes in Computer Science*, pages 334–344, 2010. doi:10.1007/978-3-642-11805-0_32.
- [70] Marcus Schaefer. *Realizability of Graphs and Linkages*, pages 461–482. Thirty Essays on Geometric Graph Theory. Springer, 2013. doi:10.1007/978-1-4614-0110-0_24.
- [71] Marcus Schaefer. Complexity of Geometric k-Planarity for Fixed k. *Journal of Graph Algorithms and Applications*, 25(1):29–41, 2021. doi:10.7155/jgaa.00548.
- [72] Marcus Schaefer and Daniel Štefankovič. Fixed Points, Nash Equilibria, and the Existential Theory of the Reals. *Theory of Computing Systems*, 60:172–193, 2017. doi:10.1007/s00224-015-9662-0.
- [73] Marcus Schaefer and Daniel Štefankovič. The Complexity of Tensor Rank. *Theory of Computing Systems*, 62(5):1161–1174, 2018. doi:10.1007/s00224-017-9800-y.
- [74] Thiago Serra, Christian Tjandraatmadja, and Srikumar Ramalingam. Bounding and Counting Linear Regions of Deep Neural Networks. In Jennifer Dy and Andreas Krause, editors, *Proceedings of the 35th International Conference on Machine Learning (ICML 2018)*, volume 80 of *Proceedings of Machine Learning Research*, pages 4558–4566, 2018.
- [75] Shai Shalev-Shwartz and Shai Ben-David. *Understanding Machine Learning: From Theory to Algorithms*. Cambridge University Press, 2014. doi:10.1017/CB09781107298019.
- [76] Yaroslav Shitov. A Universality Theorem for Nonnegative Matrix Factorizations. arXiv preprint, 2016. arXiv:1606.09068.

- [77] Yaroslav Shitov. The complexity of positive semidefinite matrix factorization. *SIAM Journal on Optimization*, 27(3):1898–1909, 2017. doi:[10.1137/16M1080616](https://doi.org/10.1137/16M1080616).
- [78] Peter W. Shor. Stretchability of Pseudolines is NP-Hard. In Peter Gritzmann and Bernd Sturmfels, editors, *Applied Geometry And Discrete Mathematics*, volume 4 of *DIMACS Series in Discrete Mathematics and Theoretical Computer Science*, pages 531–554, 1991. doi:[10.1090/dimacs/004/41](https://doi.org/10.1090/dimacs/004/41).
- [79] Matus Telgarsky. Representation Benefits of Deep Feedforward Networks. arXiv preprint, 2015. arXiv:[1509.08101](https://arxiv.org/abs/1509.08101).
- [80] Matus Telgarsky. Benefits of depth in neural networks. In Vitaly Feldman, Alexander Rakhlin, and Ohad Shamir, editors, *29th Annual Conference on Learning Theory (COLT 2016)*, volume 49 of *Proceedings of Machine Learning Research*, pages 1517–1539, 2016.
- [81] Leslie G. Valiant. A Theory of the Learnable. *Communications of the ACM*, 27(11):1134–1142, 1984. doi:[10.1145/1968.1972](https://doi.org/10.1145/1968.1972).
- [82] Gal Vardi, Gilad Yehudai, and Ohad Shamir. On the Optimal Memorization Power of ReLU Neural Networks. arXiv preprint, 2021. arXiv:[2110.03187](https://arxiv.org/abs/2110.03187).
- [83] Dmitry Yarotsky. Error bounds for approximations with deep ReLU networks. *Neural Networks*, 94:103–114, 2017. doi:[10.1016/j.neunet.2017.07.002](https://doi.org/10.1016/j.neunet.2017.07.002).
- [84] Chulhee Yun, Suvrit Sra, and Ali Jadbabaie. Small ReLU networks are powerful memorizers: a tight analysis of memorization capacity. In Hanna Wallach, Hugo Larochelle, Alina Beygelzimer, Florence d’Alché Buc, Emily Fox, and Roman Garnett, editors, *Advances in Neural Information Processing Systems (NeurIPS 2019)*, volume 32, 2019.
- [85] Chiyuan Zhang, Samy Bengio, Moritz Hardt, Benjamin Recht, and Oriol Vinyals. Understanding Deep Learning (Still) Requires Rethinking Generalization. *Communications of the ACM*, 64(3):107–115, 2021. doi:[10.1145/3446776](https://doi.org/10.1145/3446776).
- [86] Liwen Zhang, Gregory Naitzat, and Lek-Heng Lim. Tropical Geometry of Deep Neural Networks. In Jennifer Dy and Andreas Krause, editors, *Proceedings of the 35th International Conference on Machine Learning (ICML 2018)*, volume 80 of *Proceedings of Machine Learning Research*, pages 5824–5832, 2018.

A Proof of Claim 19

We prove the claim individually for each gadget type – levee, nonlinearity gadget, and cancel gadget. We first summarize the findings about required breakline locations and types from the proofs of Lemmas 10, 14 and 15 in Tables 2 to 4.

Table 2: The locations and types of breaklines in a levee.

Breakline	Location	Type
b_1	$[\ell_3, \ell_4)$	(\vee, \vee)
b_2	$(\ell_4, \ell_5]$	(\wedge, \wedge)
b_3	on ℓ_7	(\wedge, \wedge)
b_4	on ℓ_{10}	(\vee, \vee)

Table 3: The locations and types of breaklines in a nonlinearity gadget.

Breakline	Location	Type
b_1	$[\ell_3, \ell_4)$	$(\vee, 0)$
b_2	(ℓ_4, ℓ_5)	(\wedge, \vee)
b_3	$(\ell_5, \ell_6]$	$(0, \wedge)$
b_4	on ℓ_8	(\wedge, \wedge)
b_5	on ℓ_{11}	(\vee, \vee)

Table 4: The locations and types of breaklines in a cancel gadget (active in the second output dimension).

Breakline	Location	Type
b_1	$[\ell_3, \ell_4)$	$(0, \wedge)$
b_2	(ℓ_4, ℓ_5)	$(0, \vee)$
b_3	$(\ell_5, \ell_6]$	$(0, \wedge)$

Recall that every breakline has to stab exactly three breakpoint intervals. If every breakline stabs three matching breakpoint intervals, it stays between the data lines bounding these breakpoint intervals, and the breaklines can thus not intersect each other nor any data line between v_1 and v_3 .

Claim 20. *To stab all breakpoint intervals of a levee with only four breaklines, each of them has to stab three matching breakpoint intervals.*

Proof. On the three vertical lines, there are six breakpoint intervals for breaklines of type (\vee, \vee) in total. If only two breaklines should stab these six breakpoint intervals, one breakline needs to stab at least two of the single-point intervals. If a breakline goes through two of the single points, it also goes through the third point, and can thus not go through the proper intervals. Therefore one breakline must stab the single-point intervals, and the other one stabs the proper breakpoint intervals.

The same argument can be made for the breakpoint intervals of type (\wedge, \wedge) , and thus each breakline stabs three matching breakpoint intervals. \square

Claim 21. *To stab all breakpoint intervals of a nonlinearity gadget with only five breaklines, each of them has to stab three matching breakpoint intervals.*

Proof. All five sets of three matching breakpoint intervals have a different type of required breakline, thus each breakline stabs three matching breakpoint intervals. \square

Claim 22. *To stab all breakpoint intervals of a cancel gadget with only three breaklines, each of them has to stab three matching breakpoint intervals.*

Proof. There is only one set of three breakpoint intervals for a breakline of type $(0, \vee)$, so it is trivially matched correctly.

We can see that the breakpoint intervals for a breakline of type $(0, \wedge)$ have a distance of 2 from each other, and each have a width of 1. If the two breaklines of this type would not stab three matching breakpoint intervals, one of them would need to stab two matching intervals and one non-matching interval. As the distance between the vertical lines is equal and the breakpoint intervals are further apart from each other than their width, there is no way for a breakline to lie in this way.

We conclude that all breaklines stab three matching breakpoint intervals. \square

We have proven Claim 19 for each gadget type individually, and thus the claim holds.